AD-A191 977 CURRENTS INDUCED IN A HUMAN BEING FOR ELECTROMAGNETIC FIELDS 10 KHZ-50 MHZ(U) UTAH UNIV RESEARCH INST SALT LAKE CITY O P GANDHI 15 JAN 88 ETL-88002-TR 1/1

UNCLASSIFIED N00014-86-K-0104 F/G 6/10 NL

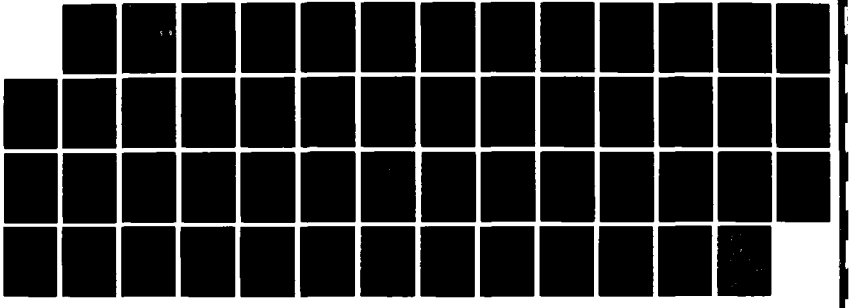

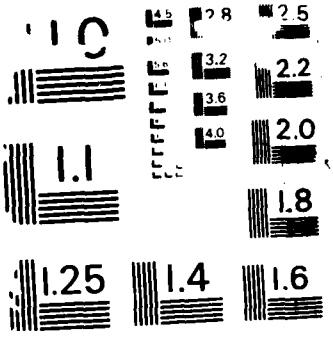

RESOLUTION TEST CHART
NATIONAL BUREAU OF STANDARDS - 1963

ETL-88002-TR

University of Utah Research Institute
391 Chipeta Way, Suite C
Salt Lake City, Utah 84108-1295

Naval Medical R & D Command
NMC - NCR
Bethesada, Maryland, 20814-5044

Attn: Capt. W. M. Houk

Final Report on Project

N 00014-86-K 0104

CURRENTS INDUCED IN A HUMAN BEING FOR ELECTROMAGNETIC FIELDS 10 kHz-50 MHz

Principal Investigator

Om P. Gandhi

January 15, 1988

CURRENTS INDUCED IN A HUMAN BEING FOR ELECTROMAGNETIC FIELDS 10KHz - 50 MHz

Introduction

We have previously shown [1, 2] that vertically polarized incident plane waves are capable of inducing fairly significant RF currents in a free-standing human being. Foot currents were found to be proportional to the frequency of incident radiation for the frequency band 0-40 MHz with values as high as 12.7 mA/(V/m) measured for adult human volunteers at 40 MHz. This work has pointed to the possibility of large induced currents estimated to be on the order of 627.4 mA for the ANSI recommended [3] 3-30 MHz RF safety level -- RMS incident electric field $E = 1897/f_{MHz}$, with current values peaking at 780 mA for the ANSI recommended $E = 61.4$ V/m (1 mW/cm^2) at 40 MHz. Recognizing that the induced current is divided equally between the two legs on its way to the ground underneath, fairly high current densities result in the various cross sections of the leg with concommitant high rates of energy deposition (SAR). In particular, due to the predominantly bony nature of the ankle cross section forcing the RF current to flow in an effective 9.5 cm^2 cross section of the high conductivity tissues, very high current densities (J) and the resulting SARs are set up. For the ANSI-recommended electric fields, current densities and SARs calculated for the ankle section are: 1. for 3-30 MHz band, $J = 33$ mA/cm^2, SAR = 182 W/kg and 2. for f = 40 MHz, $J = 41$ mA/cm^2, SAR = 243 W/kg. These SARs are almost two orders of magnitude larger than the metabolic rates of the tissues and considerably in excess of the ANSI guideline [3] of 8 W/kg for any 1 g of tissue.

The two tasks undertaken during the period of this project are:

1. Development of a high resolution thermal model of the human leg and its use to estimate the temperature distribution as a result of the induced high current densities at radio frequencies.
2. Development of a high-resolution, anatomically-realistic, inhomogeneous model of man and its use to calculate the SAR and induced current distributions for frequencies to 100 MHz.

TEMPERATURE DISTRIBUTIONS IN THE HUMAN LEG FOR VLF-VHF EXPOSURES AT THE ANSI-RECOMMENDED SAFETY LEVELS

This work is detailed in Appendix A which has been submitted for possible publication to IEEE Transactions on Biomedical Engineering.

Using a block model of 1,532 cubical cells, temperature distributions are calculated for the lowest 21 cm of the human leg for electric fields recommended in the ANSI RF safety guideline. The thermal model uses inhomogeneous volume-averaged tissue properties: blood-flow rate, metabolism, thermal conductivity, specific heat, etc. The SARs are obtained using the impedance method. A modified method of finite difference technique is used to solve the 3-D heat conduction equation for the thermal model. Numerical results are obtained for RF currents at 3 and 40 MHz projected for the E-fields recommended by the ANSI Standard (614 and 61.4 V/m, respectively) and also for power densities one-tenth of that level. Temperatures as high as 41.6° are obtained for some internal cells for the higher E-fields while relatively moderate temperatures on the order of 37° C are obtained for the lower E-fields. Some of the calculated results for the surface temperature have been compared and found to be in good agreement with the experimental data for initial rates of heating.

AN ANATOMICALLY-BASED MODEL OF MAN AND ITS USE FOR SAR AND INDUCED CURRENT DISTRIBUTIONS

Similar to references [4] and [5], the inhomogeneous model of the human body is based on the anatomical cross sections given in the book, "A Cross-Section Anatomy," by Eycleshymer and Schoemaker [6]. This book contains cross-sectional diagrams of the human body which were obtained by making cross-sectional cuts at spacings of about one inch in human cadavers. The process for creating the data base of the man model was the following: first of all a quarter-inch grid was taken for each single cross-sectional diagram and each cell on the grid was assigned a number corresponding to one of the 14 tissue types given in Table 1. Thus the data associated with a particular layer consisted of three numbers for each square cell: x and y positions relative to same anatomical reference point in this layer, usually the center of the spinal cored, and an integer indicating which tissue that cell contained. Since the cross-sectional diagrams available in reference [6] are for somewhat variable separations typically 2.3-2.7 cm, a

new set of equispaced layers were defined at 1/4" intervals by interpolating the data onto these layers. Since the cell size of quarter-inch is too small for the memory space of present day computers, the proportion of each tissue type was calculated next for somewhat larger cells of size one inch by combining the data for 4 x 4 x 4 = 64 cells of the smaller dimension. Without changes in the anatomy, this process allows some variability in the height and weight of the body. We have taken the final cell size of 2.62 cm (rather than 1" or 2.54 cm) to obtain the whole-body weight of 69.6 kg for the model.

The finite-difference tissue-domain method described in our earlier publications [4,5] has been used to calculate the internal electric fields (E) for the model of man subjected to vertically-polarized plane waves at frequencies between 20 and 100 MHz. The model is assumed to be nestled in a rectangular volume of 38 x 26 x 84 or 82,992 cells of dimensions 2.62 cm on each of the sides. The electromagnetic fields are calculated using CRAY XMP computer requiring cpu times on the order of 2.5 - 5 minutes, depending upon the frequency. Both isolated and grounded conditions are used for the calculations. The local SARs are calculated from the relationship SAR = $\sigma \vec{E} \cdot \vec{E}/2\rho'$ where σ is the electrical conductivity and ρ the mass density obtained for the individual cubical cell from the volume-averaged properties of the respective tissues contained therein. The layer-averaged values of SARs calculated for incident plane waves of power density 1 mW/cm^2 (incident E-field of 61.4 V/m) are shown in Figs. 1-10 for isolated and grounded conditions for frequencies 20-100 MHz. Lower frequencies have not been used for calculations since the SARs are considerably lower at these frequencies.

The whole-body-averaged SARs for grounded and isolated man models are shown in Fig. 11 for various frequencies. Also shown for comparison is the experimental data by Guy and Chou [7]. Whereas these authors have used scaled, homogeneous models with conductivity corresponding to 2/3 that for muscle, an anatomically-based inhomogeneous model has been used for the present calculations. It is interesting to note that the SARs given by the inhomogeneous model are significantly higher than those obtained for the homogeneous model. As will be seen later (Figs. 13 - 22) substantial radio frequency currents are induced in the legs. Because of the large bone content of the legs, an inhomogeneous model properly accounts for the lower effective conductivities for this region, which therefore results in higher SARs.

From Figs. 1-10 it may be seen that the highest SARs are calculated for the sections through the neck, the knee and the ankle - the former being due to a smaller cross section and the latter two due to the high bone content as well. The layer-averaged SARs for ankle- , knee-, and neck sections calculated for grounded and isolated conditions are shown in Fig. 12.

We have used the internal E-fields to calculate the local current densities from the relationship $\vec{J} = (\sigma + j\omega\varepsilon)\vec{E}$. The z-directed currents for any of the layers are obtained by summing up the terms due to the individual cells in a given layer as follows:

$$I = \Delta^2 \sum_i \left(\sigma_i + j\omega\varepsilon_i\right) E_{zi} \tag{1}$$

where Δ^2 is the cross sectional area (2.62 x 2.62 cm^2) for each of the cells.

The layer-averaged induced current distributions are shown in Figs. 13-22 for isolated and grounded conditions for frequencies of 27-90 MHz. Since E-fields of 61.4 V/m have been recommended as safe in the ANSI C95.1 - 1982 RF safety guideline [3] for the frequency band 30-300 MHz, substantial RF induced currents are obviously implied from the data given in Figs. 13-22. A comparison is made in Fig. 23 of the foot currents calculated for a grounded model to those that were measured by Gandhi, et al. [2] using human subjects. Somewhat lower currents are obtained from the model calculations than were measrued experimentally [2]. This may be due to the relative crudeness of the present model. Finer models using smaller cell sizes would provide better representation of reality and may result in giving a better agreement with the measured data.

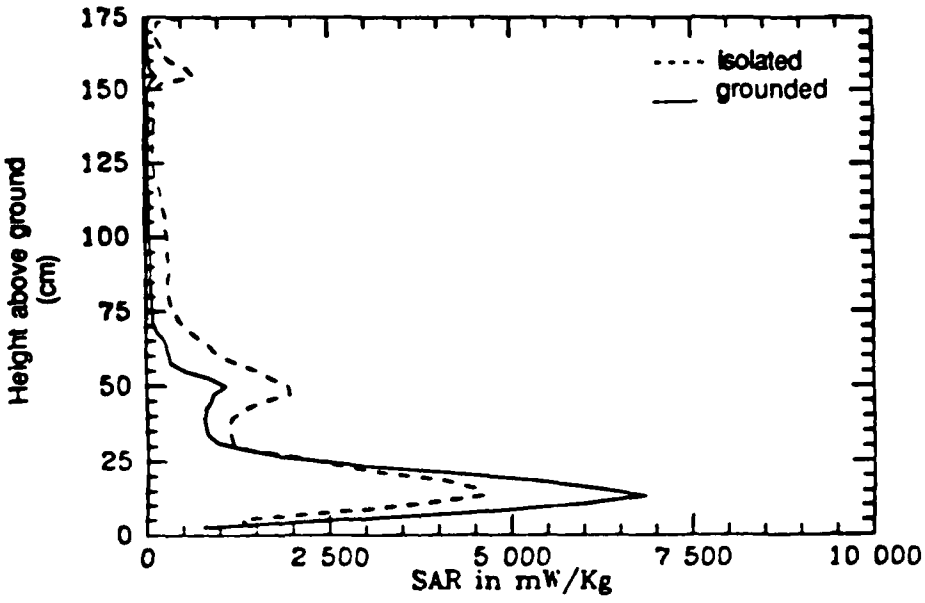

Fig. 1. Layer-averaged SAR distributions for a grounded and isolated man model at 20 MHz. All SARs are the result of 1 $\frac{mW}{cm^2}$ incident plane-wave. The SARs for the isolated man model have been multiplied by 10.

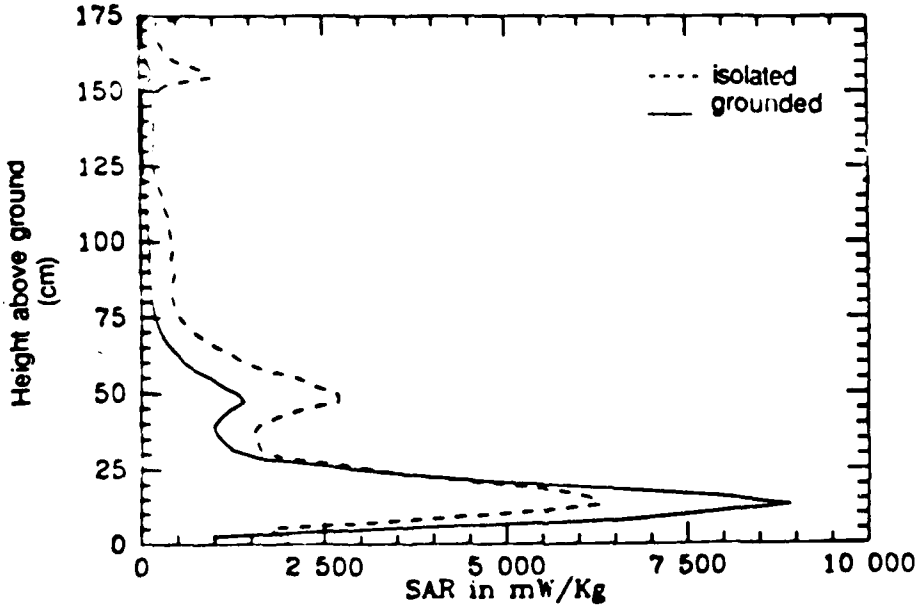

Fig. 2. Layer-averaged SAR distributions for a grounded and isolated man model at 27 MHz. All SARs are the result of 1$\frac{mW}{cm^2}$ incident plane-wave. The SARs for the isolated condition have been multiplied by 10.

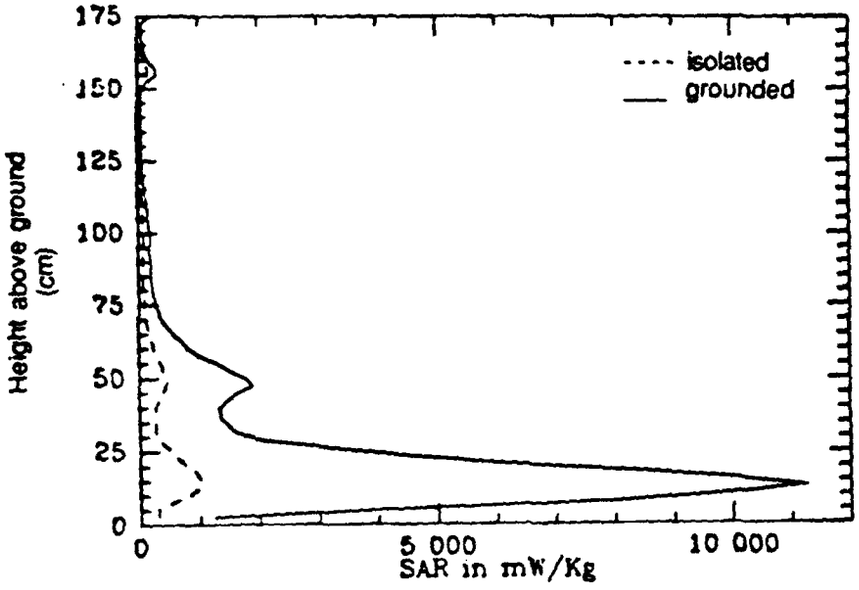

Fig. 3. Layer-averaged SAR distributions for a grounded and isolated man model at 40 MHz. All SARS are the result of $1\frac{mW}{cm^2}$ incident plane-wave.

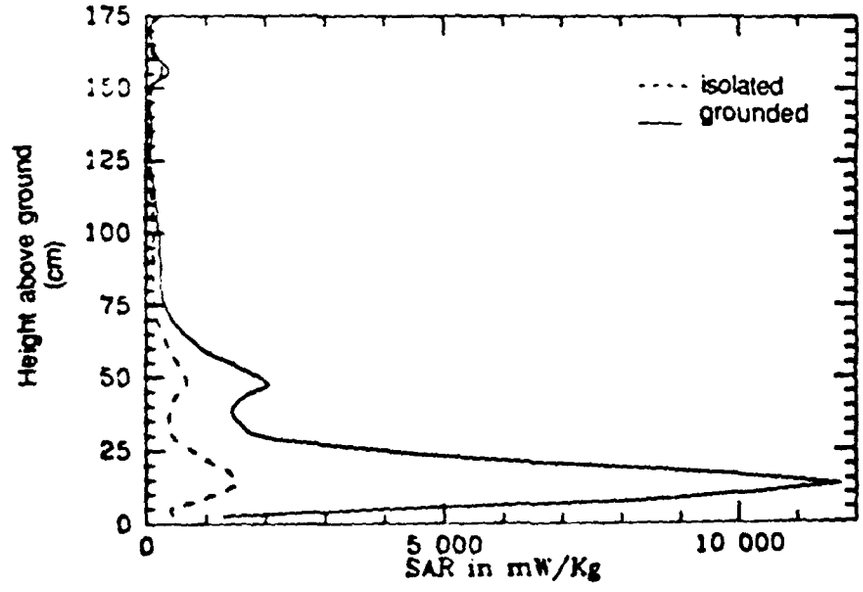

Fig. 4. Layer-averaged SAR distributions for a grounded and isolated man model at 45 MHz. All SARs are the result of $1\frac{mW}{cm^2}$ incident plane-wave.

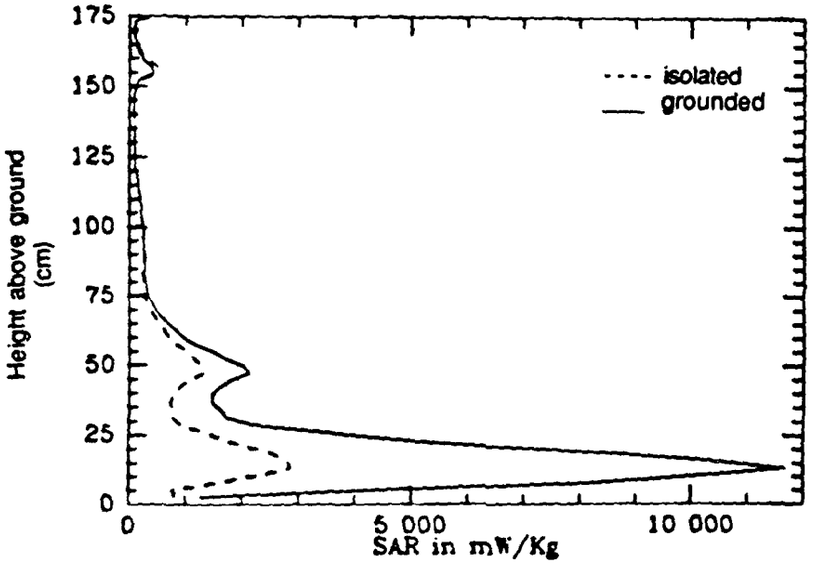

Fig. 5. Layer-averaged SAR distributions for a grounded and isolated man model at 50 MHz. All SARs are the result of $1\frac{mW}{cm^2}$ incident plane-wave.

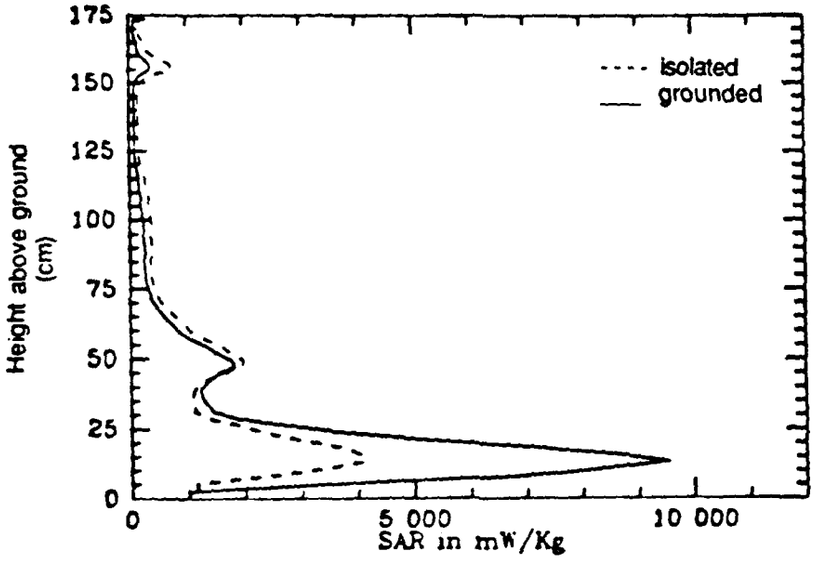

Fig. 6. Layer-averaged SAR distributions for a grounded and isolated man model at 55 MHz. All SARs are the result of $1\frac{mW}{cm^2}$ incident plane-wave.

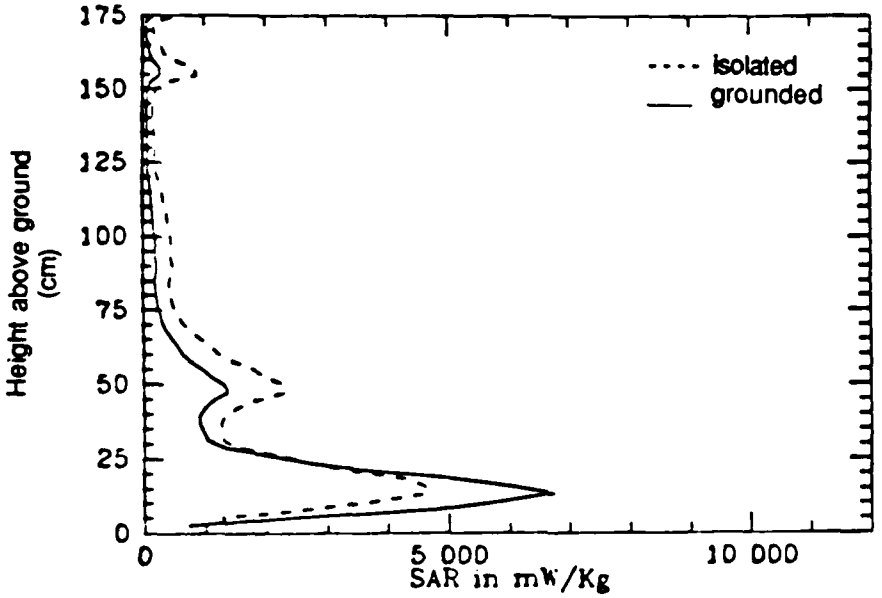

Fig. 7. Layer-averaged SAR distributions for a grounded and isolated man model at 60 MHz. All SARs are the result of $1\frac{mW}{cm^2}$ incident plane-wave.

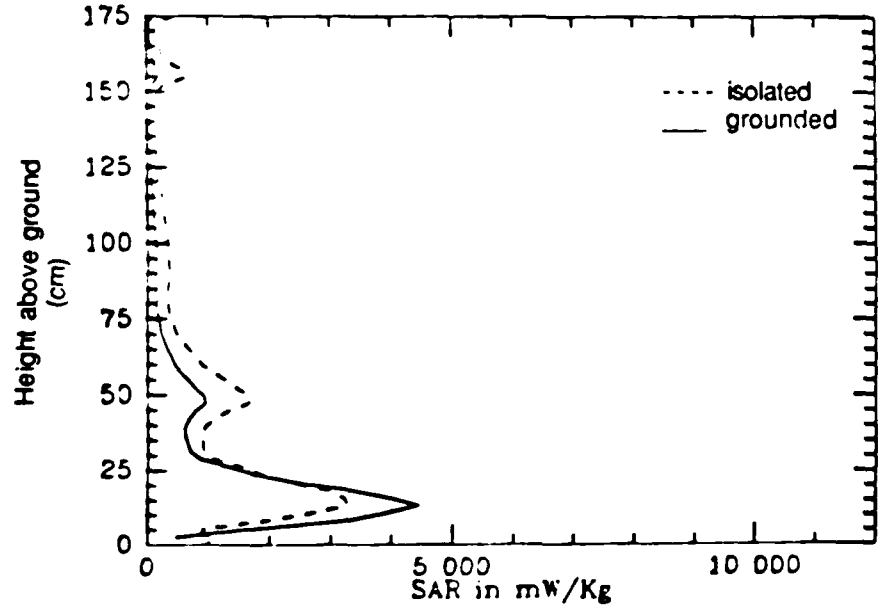

Fig. 8. Layer-averaged SAR distributions for a grounded and isolated man model at 65 MHz. All SARs are the result of $1\frac{mW}{cm^2}$ incident plane-wave.

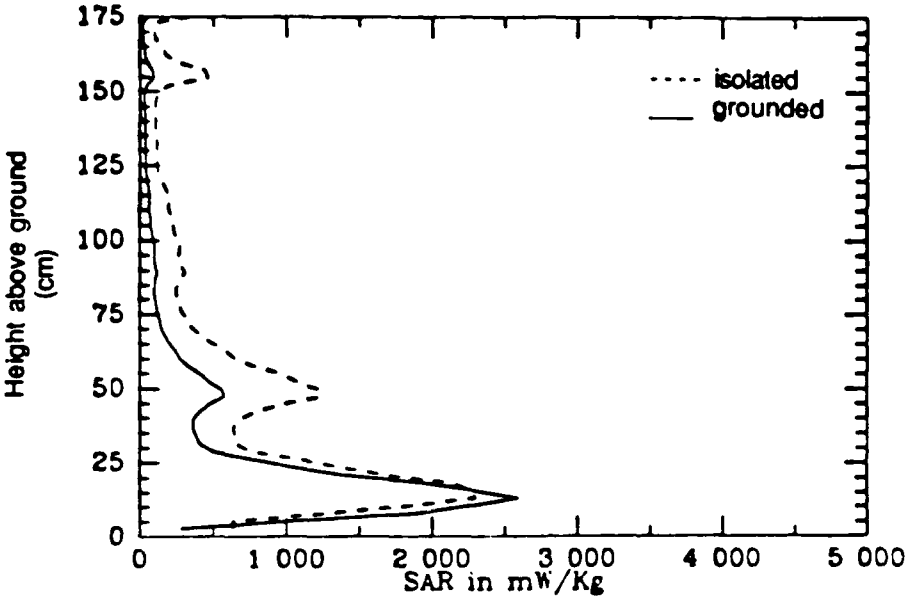

Fig. 9. Layer-averaged SAR distributions for a grounded and isolated man model at 70 MHz. All SARs are the result of $1\frac{mW}{cm^2}$ incident plane-wave.

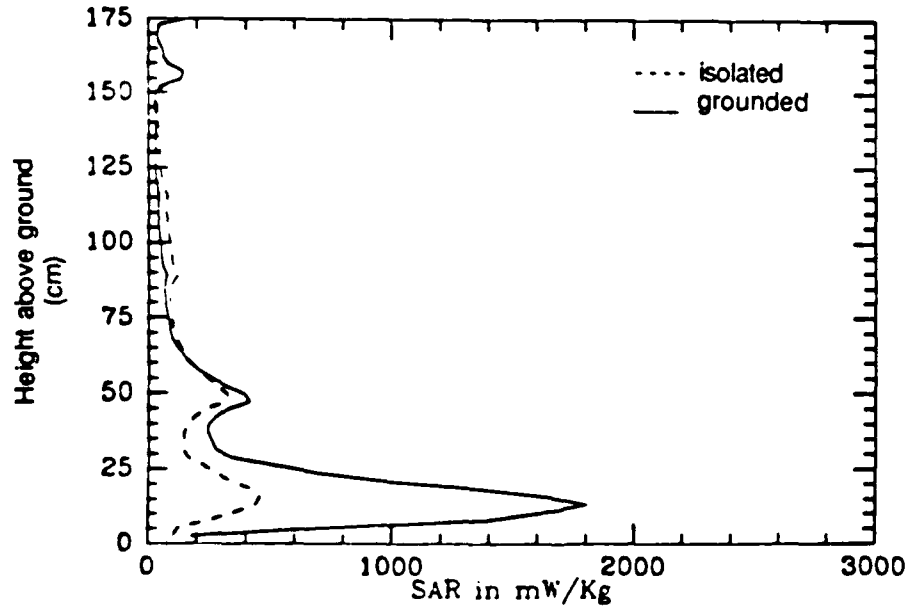

Fig. 10. Layer-averaged SAR distributions for a grounded and isolated man model at 100 MHz. All SARs are the result of $1\frac{mW}{cm^2}$ incident plane-wave.

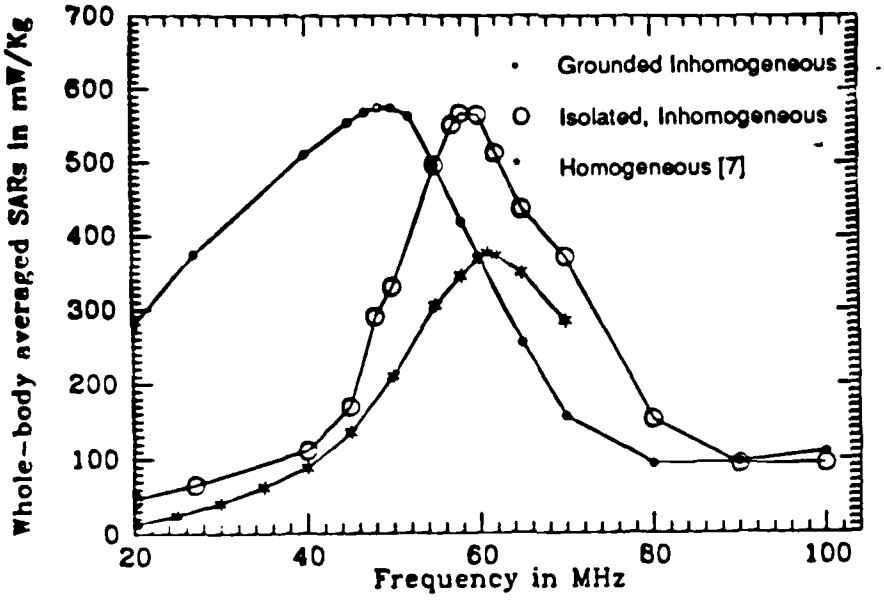

Fig. 11. Whole-body averaged SARs for a grounded and isolated man model. Also shown for comparison is the homogeneous, isolated model data of Guy and Chou [7].

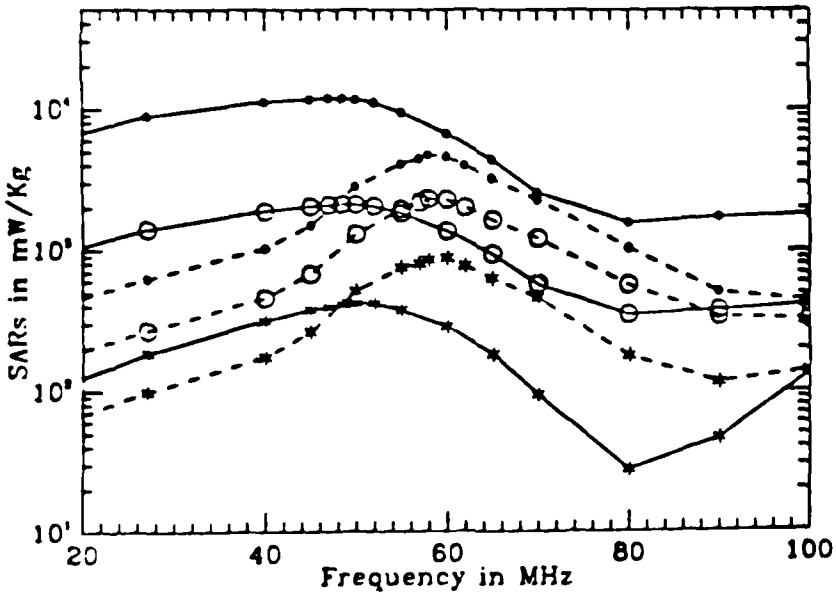

Fig. 12. Layer-averaged SARs for ankle-, knee- and neck sections under grounded and isolated conditions. All SARs are the result of 1 $\frac{mW}{cm^2}$ incident plane-wave.

• ankle section; o: knee section *: neck section

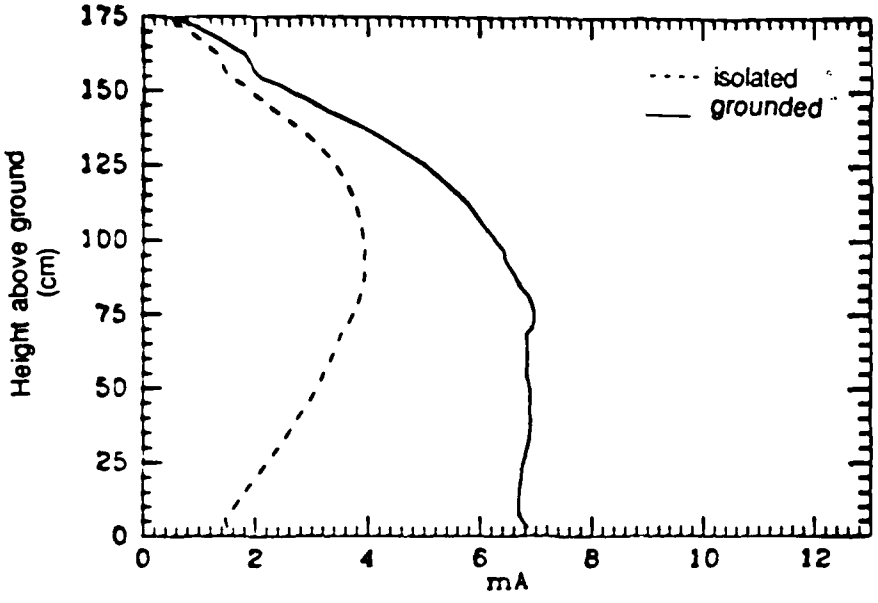

Fig. 13. Induced RF current distributions for a grounded and isolated man model at 27 MHz for incident 1 V/m plane-wave exposure condition.

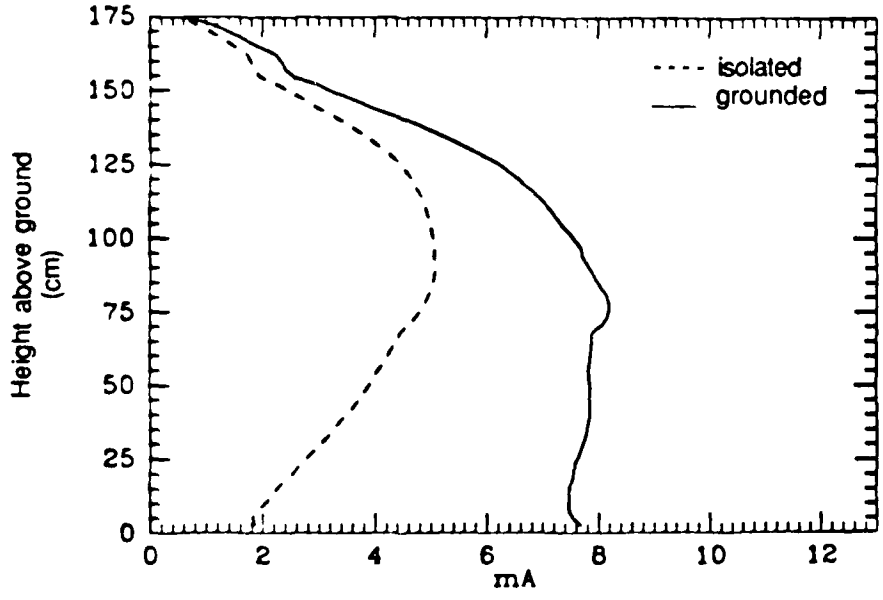

Fig. 14. Induced RF current distributions for a grounded and isolated man model at 35 MHz for incident 1 V/m plane-wave exposure condition.

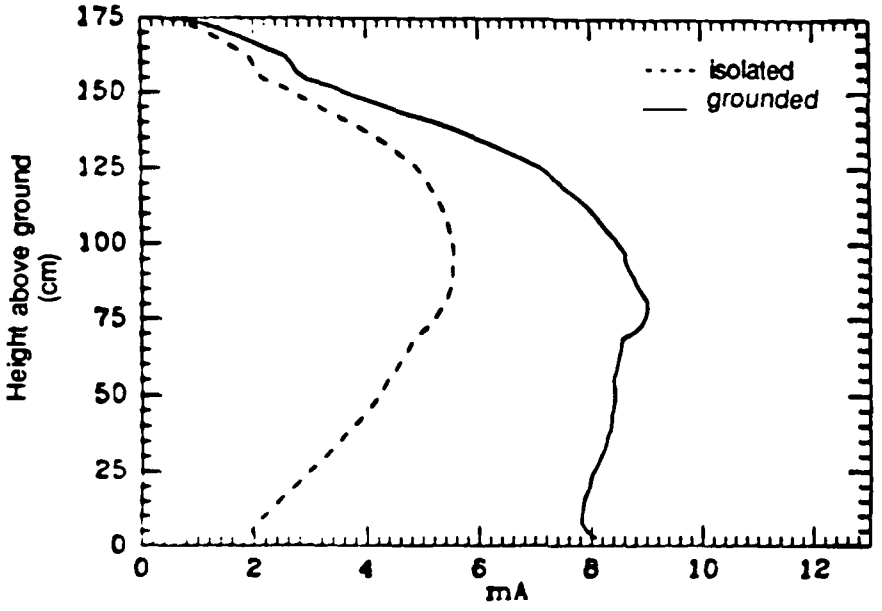

Fig 15. Induced RF current distributions for a grounded and isolated man model at 40 MHz under 1 V/m plane-wave exposure condition.

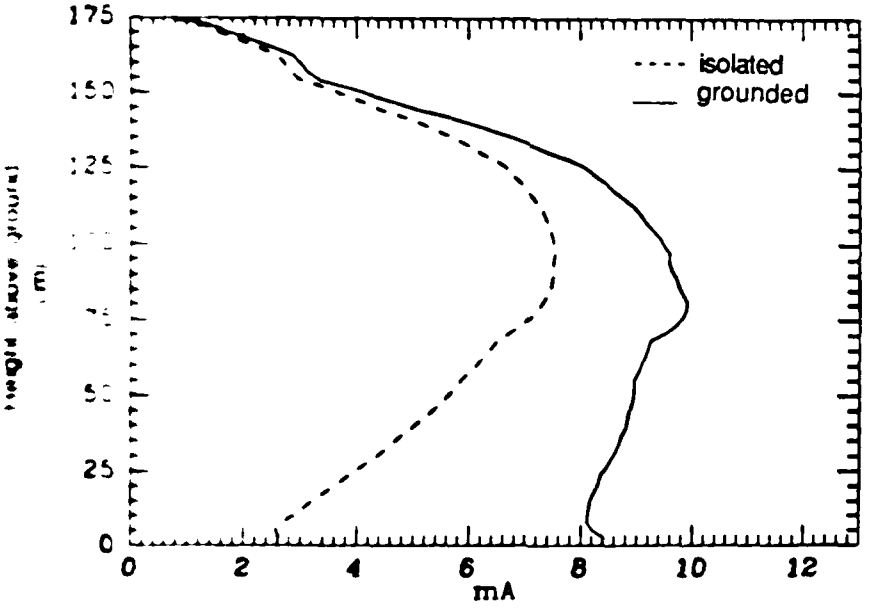

Fig 16 Induced RF current distributions for a grounded and isolated man model at 45 MHz under 1 V/m plane-wave exposure condition.

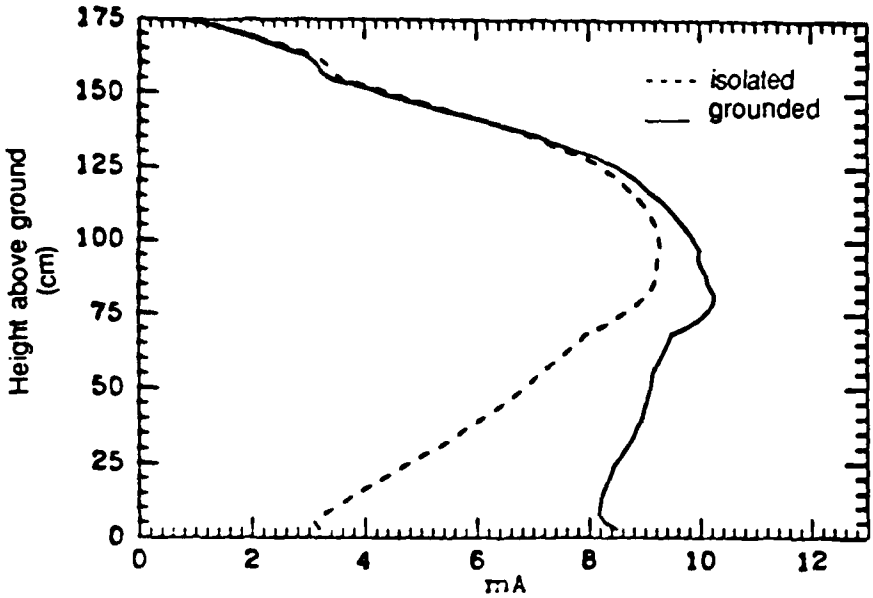

Fig. 17. Induced RF current distributions for a grounded and isolated man model at 48 MHz under 1 V/m plane-wave exposure condition.

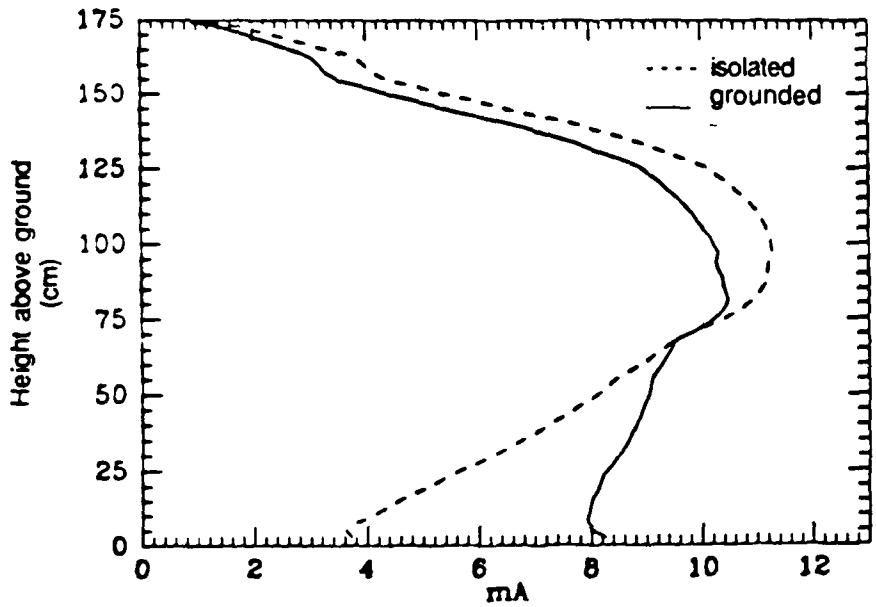

Fig. 18. Induced RF current distributions for a grounded and isolated man model at 52 MHz under 1 V/m plane-wave exposure condition.

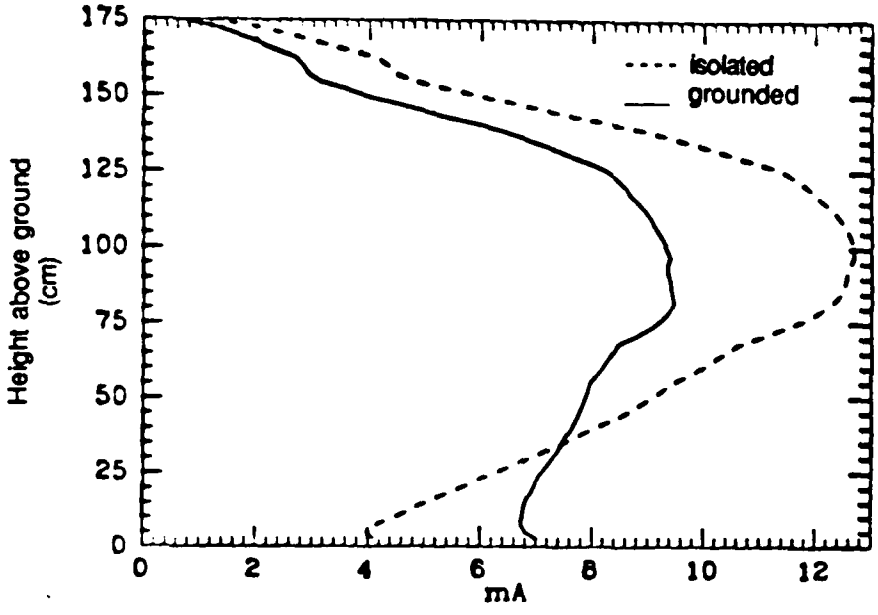

Fig. 19. Induced RF current distributions for a grounded and isolated man model at 58 MHz under 1 V/m plane-wave exposure condition.

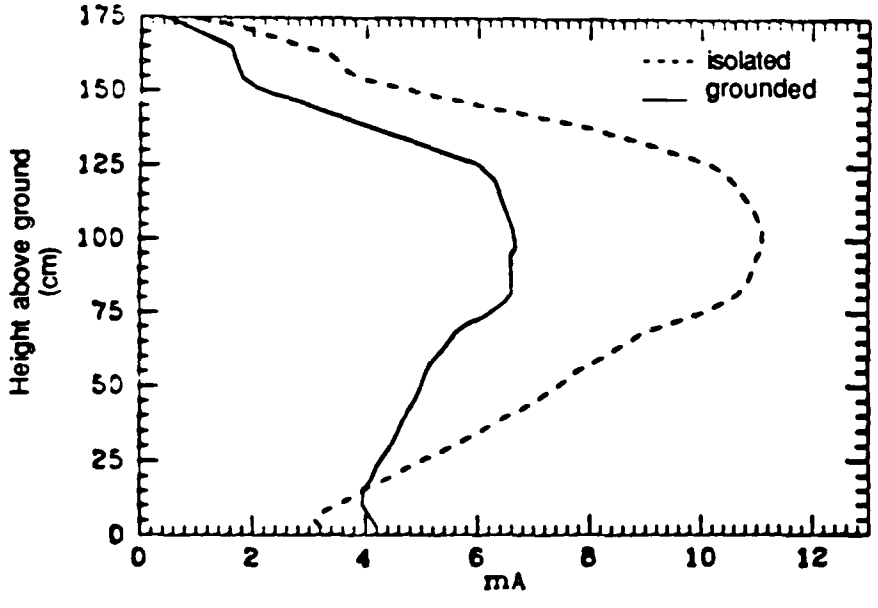

Fig. 20. Induced RF current distributions for a grounded and isolated man model at 70 MHz under V/m plane-wave exposure condition.

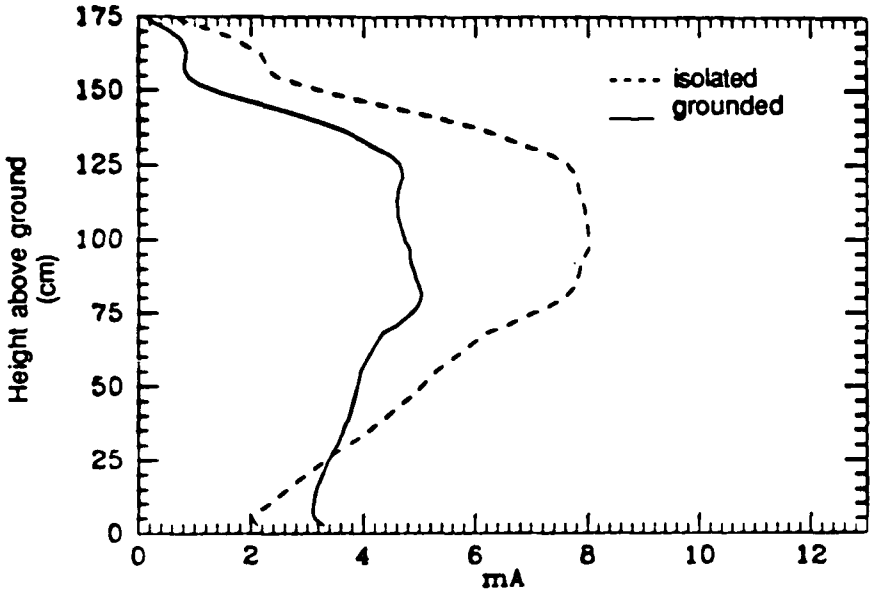

Fig. 21. Induced RF current distributions for a grounded and isolated man model at 80 MHz under 1 V/m plane-wave exposure condition.

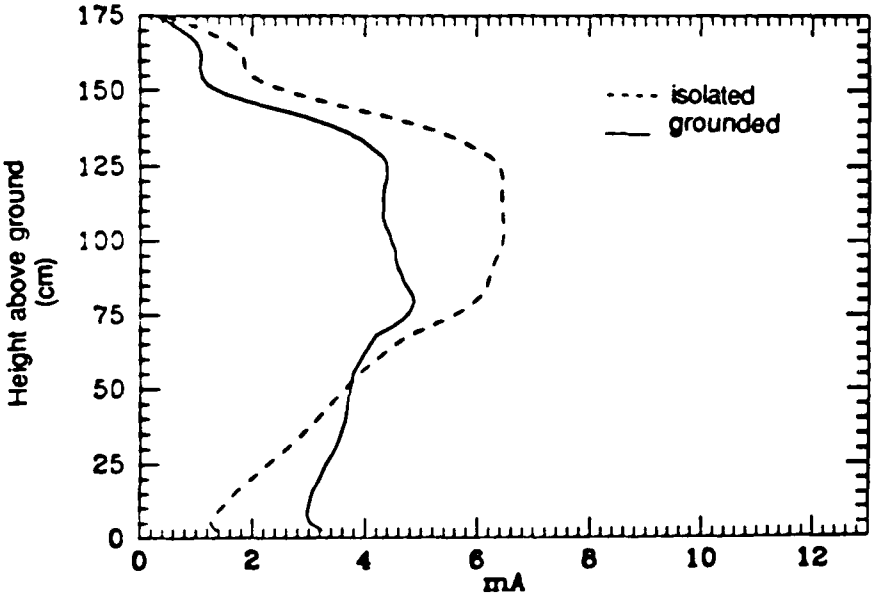

Fig. 22. Induced RF current distributions for a grounded and isolated man model at 90 MHz under 1 V/m plane-wave exposure condition.

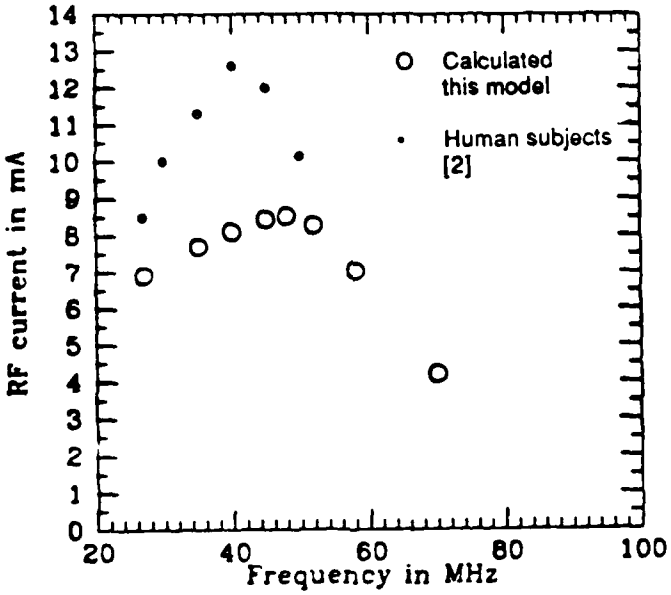

Fig. 23. Comparison of RF foot currents calculated for a grounded man model with those measured for human subjects [2]. E_{inc} = 1 V/m.

Table 1.
Tissue properties used for the man model.

Tissues Type	Mass Density ρ	20 MHz		27 MHz		40 MHz		45 MHz	
	1000 Kg/m^3	σS/m	ε_r	σS/m	ε_r	σS/m	ε_r	σS/m	ε_r
air	0.0012	0.0	1.0	0.0	1.0	0.0	1.0	0.0	1.0
muscle	1.05	0.62	132	0.74	106	0.77	92	0.77	90
fat, bone	1.20	0.04	29	0.04	29	0.04	22	0.04	19
blood	1.00	0.28	130	0.28	102	0.48	93	0.56	90
intestine	1.00	0.25	61	0.29	60	0.32	53	0.32	50
cartilage	1.00	0.04	29	0.04	29	0.04	22	0.04	19
liver	1.03	0.50	150	0.51	132	0.54	115	0.55	108
kidney	1.02	0.64	220	0.79	209	0.84	170	0.86	159
pancreas	1.03	0.62	220	0.69	206	0.74	175	0.75	164
spleen	1.03	0.62	220.	0.69	206	0.74	175	0.75	164
lung	0.33	0.22	46	0.17	34	0.20	31	0.21	30
heart	1.03	0.52	230	0.64	210	0.66	164	0.66	148
nerve, brain	1.05	0.30	160	0.45	155	0.46	132	0.46	124
skin	1.00	0.62	132	0.74	106	0.77	92	0.77	87
eye	1.00	0.30	160	0.45	155	0.46	132	0.46	124

* We have used 33 percent lung tissue and 67 percent air for the dielectric properties of the lung.

Table 1. (continued)
Tissue properties used for the man model.

Tissues Type	50MHz		55 MHz		60 MHz		65 MHz		70 MHz		100MHz	
	σS/m	ε_r	σS/m	ε_r	σS/m	ε_r	σS/m	ε_r	σS/m	ε_r	σS/m	ε_r
air	0.0	1.0	0.0	1.0	0.0	1.0	0.0	1.0	0.0	1.0	0.0	1.0
muscle	0.78	89	0.79	87	0.80	86	0.84	84	0.88	83	1.0	74
fat, bone	0.05	16	0.05	11	0.06	8.5	0.06	8.3	0.06	8.2	0.07	7.5
blood	0.64	87	0.72	88	0.80	80	0.84	79	0.88	78	1.1	74
intestine	0.33	47	0.34	43	0.35	40	0.38	39	0.42	38	0.55	36
cartilage	0.05	16	0.05	11	0.06	8.5	0.06	8.3	0.06	8.2	0.07	7.5
liver	0.56	102	0.57	95	0.58	88	0.59	87	0.59	85	0.62	77
kidney	0.87	148	0.88	132	0.90	115	0.91	111	0.93	109	1.0	90
pancreas	0.77	153	0.78	142	0.80	130	0.81	125	0.83	120	1.0	90
spleen	0.77	153	0.78	142	0.80	130	0.81	125	0.80	122	0.82	100
lung	0.22	29	0.23	28	0.24	27	0.26	26	0.28	26	0.34	75
heart	0.67	132	0.67	108	0.68	100	0.69	97	0.70	94	0.75	76
nerve, brain	0.46	116	0.46	108	0.47	100	0.48	97	0.49	95	0.53	82
skin	0.78	82	0.79	77	0.80	72	0.80	66	0.80	60	0.55	25
eye	0.46	116	0.46	108	0.47	100	0.64	98	0.80	96	1.9	85

* We have used 33 percent lung tissue and 67 percent air for the dielectric properties of the lung.

REFERENCES

1. O. P. Gandhi, I. Chatterjee, D. Wu, and Y. G. Gu, "Likelihood of High Rates of Energy Deposition in the Human Legs at the ANSI Recommended 3-30 MHz RF Safety Levels," *Proceedings of the IEEE*, Vol. 73, 1985, pp. 1145-1147.

2. O. P. Gandhi and J. Y. Chen, "Currents Induced in a Human Being for Plane-Wave Exposure Conditions 0-50 MHz and for RF Sealers," *IEEE Transactions on Biomedical Engineering*, Vol. BME-33, 1986, pp. 486-494.

3. ANSI C95.1-1982, "American National Standard -- Safety Levels with Respect to Human Exposure to Radio-Frequency Electromagnetic Fields, 300 kHz to 100 GHz," printed by the Institute of Electrical and Electronics Engineers, Inc., 345 East 47th Street, New York, New York, 10017.

4. D. M. Sullivan, D. T. Borup and O. P. Gandhi, "Use of the finite-difference time-domain method in calculating absorption in human tissues," *IEEE Transactions on Biomedical Engineering*, Vol. BME-34, 1987, pp. 148-157.

5. D. M. Sullivan, O. P. Gandhi and A. Taflove, "Use of the finite-difference time-domain method in calculating EM absorption in man models," *IEEE Transaction on Biomedical Engineering*, Vol. BME-35, March 1988.

6. A. C. Eycleshymer and D. M. Shoemaker, "A Cross-Section Anatomy," D. Appleton and Company, New York and London, 1911.

7. A. W. Guy and C. K. Chou,"Hazard Analysis: Very low frequency through medium frequency range," Final Report USAF SAM Contract F33615-78-D-0617 Task 0065, February 1982.

APPENDIX A

TEMPERATURE DISTRIBUTIONS IN THE HUMAN LEG FOR VLF-VHF EXPOSURES AT THE ANSI-RECOMMENDED SAFETY LEVELS

M. Hoque and Om P. Gandhi
Electrical Engineering Department
University of Utah
Salt Lake City, Utah 84112

Accepted for publication IEEE Transactions on Biomedical Engineering.

ABSTRACT

Using a block model of 1532 cubical cells, temperature distributions are calculated for the lowest 21 cm of the human leg for electric fields recommended in the ANSI RF safety guideline. The thermal model uses inhomogeneous volume-averaged tissue properties: blood-flow rate, metabolism, thermal conductivity, specific heat, etc. The SARs are obtained using the impedance method. A modified method of finite difference technique is used to solve the 3-D heat conduction equation for the thermal model. Numerical results are obtained for RF currents at 3 and 40 MHz projected for the E-fields recommended by the ANSI Standard (614 and 61.4 V/m, respectively) and also for power densities one-tenth of that level. Temperatures as high as 41.6° are obtained for some internal cells for the higher E-fields while relatively moderate temperatures on the order of 37°C are obtained for the lower E-fields. Some of the calculated results for the surface temperature have been compared and found to be in good agreement with the experimental data for initial rates of heating.

I. INTRODUCTION

The present radio frequency RF radiation standards suggested by American National Standards Institute (ANSI) and the American Conference of Government Industrial Hygienists are based on the knowledge of whole-body-average specific absorption rate (SAR) [1,2]. For the electric fields recommended in the ANSI C95.1-1982 RF Safety Guide, fairly high SARs have been projected for the high-water-content tissues of the ankle section. The SARs are estimated to be on the order of 182 W/kg for the frequency band 3-30 MHz rising to a value of 243 W/kg at 40 MHz for E=61.4 V/m. The corresponding current through each of the legs is estimated to be 314 mA and 390 mA, respectively [3,4]. Our present study determines the temperature distributions of the lowest portion of the leg under these conditions. For this purpose inhomogeneous electromagnetic and thermal models are developed for the lowest 21 cm of the human leg.

Temperature distribution in different parts of the human body under EM exposure is of basic interest for radio frequency hazards analyses. The thermal models in existence to date are capable of giving only averaged temperature over large regions of the body. The most useful and detailed thermoregulatory models used to date are based on a cylindrical thermal model described by Stolwijk [5-7]. Later several modified versions of this model were developed by Wissler [8,9]. Lastly, a 476-block thermal model was developed by Chatterjee and Gandhi [10]. This thermal model used Hagmann's [11] 180-cell block model of man for electromagnetic energy deposition. Recently, a 41,000 cell

model of man has been developed for SAR calculations by Sullivan, Gandhi and Taflove using finite-difference time-domain technique [12]. In this study we have used an impedance method for detailed SAR calculations. The SARs thus determined are used in the thermal block model to find the internal temperature distribution. For temperature calculations, the lowest 21 cm section of the leg, as shown in the insertion in Fig. 2, is modeled by 1532 cubical cells each of size 1 x 1 x 1 cm.

II. THE ELECTROMAGNETIC MODEL FOR ENERGY DEPOSITION IN THE LEG SECTION.

The model for calculations of specific absorption rates (SARs) is developed with 21 transverse sections of 1 cm thickness (see the insert in Fig. 2). For each section the tissue types are determined with a resolution of 1 mm^2. The individual sections of the model are collected from the literature on the human anatomy [13]. The model is based on equipotential concept. Each section is assumed to be an equipotential; i.e., no lateral flow of current is supposed to exist. This concept can be justified from the fact that for highly-conducting tissues (at VLF-VHF frequencies) the potential gradient exists mainly along the axial direction of the model. This results in a current primarily along the axial direction. Also, because of the large wavelength of the radiation no appreciable gradient along the transverse direction of the model exists. As a result the equivalent impedance for each section is composed of parallel combination of the impedances obtained from the ten tissue types as shown [14,15,16] in Table 1.

Finally, the complete impedance of the model is the series

Table 1. Dielectric properties of the different tissue types.

Tissue types	Tissue type No. i	f = 3 MHz		f = 40 MHz	
		Dielectric constant ε_i	Conductivity σ S/m	Dielectric constant ε_i	Conductivity σ S/m
Fat/yellow marrow	1	33.0	0.051	29.0	0.04
Muscle	2	107.0	0.8	96.0	0.8
Red marrow	3	231.0	0.3	138.2	0.43
Tendon/connective tissue	4	6.5	0.0001	6.5	0.0001
Tendon and fat	5	20.0	0.0195	12.11	0.0259
Bone	6	26.0	0.015	15.47	0.027
Skin	7	108.0	0.62	108.0	0.62
Blood	8	80.0	1.1	80.0	1.1
Synovial fluid	9	95.0	1.1	95.0	1.1
Periostium	10	95.0	1.1	95.0	1.1

summation of the individual impedances for each of the sections. The electromagnetic energy deposited in different tissues of each section can be obtained from the corresponding impedances and currents. Mathematically this may be done as follows,

$$Z_{ij} = (\sigma_i - j\omega\varepsilon_i)\, L/[(\sigma_i^2 + \omega^2\, \varepsilon_i^2)A_{ij}] \qquad (1)$$

$$Y_{ij} = (\sigma_i + j\omega\, \varepsilon_i)\, A_{ij}/L \qquad (2)$$

where

Z_{ij} = Impedance of the ith tissue in the jth section

Y_{ij} = Admittance of the ith tissue in the jth section

A_{ij} = Area of the ith tissue in the jth section

σ_i = Conductivity of the ith tissue

ε_i = Electrical permittivity of the ith tissue

L = Thickness for each of the sections (assumed to be 10^{-2} m).

Power P_{ij} absorbed in $Z_{ij} = I_{ij}\, I_{ij}^{*}\, \mathrm{Re}\,(Z_{ij})$

$$= \frac{I_T\, I_T^{*}\, \sigma_i\, A_{ij}}{\sum_{i=1}^{10} \frac{1}{Z_{ij}} \sum_{i=1}^{10} \frac{1}{Z^{*}_{ij}}\, L}$$

$$Z_{tj} = 1/\sum_{i=1}^{10} Y_{ij} \qquad (3)$$

For the complete model the total values can also be written:

$$Z_T = \sum_{j=1}^{21} Z_{tj}$$

$$P_T = I_T \, I_T^* \, \mathrm{Re}\,[Z_T] \qquad (4)$$

where,

I_T = Total current flowing through the leg section,

I_{ij} = Current flowing through the ith tissue of the jth section,

P_{ij} = EM energy deposited in the ith tissue of the jth section,

Z_{tj} = Total impedance for the jth section,

Z_T = Total impedance of the model,

P_T = Total EM energy deposited in the model.

Total impedance of the model is calculated and found to be 104 Ω and 85 Ω at 3 MHz and 40 MHz, respectively. These results are consistent with the experimental values [17]. The small discrepancies in the impedances are because of the discretization of the leg section into finite segments.

The electromagnetic energy deposited is thus calculated in the individual sections for each of the tissue types. The layer-average SARs calculated for the various sections are shown in Fig. 1. The figure indicates that the highest EM energy is deposited near the ankle region where highly-conducting tissues like periostium, synovial fluid and red marrow are present. It may be noted here that Fig. 1 indicates the average SAR values in individual layers, while in reality very high SARs (of the order of 150 W/kg) in the conducting tissues in some of the sections (near the ankle region) are obtained with a resolution of

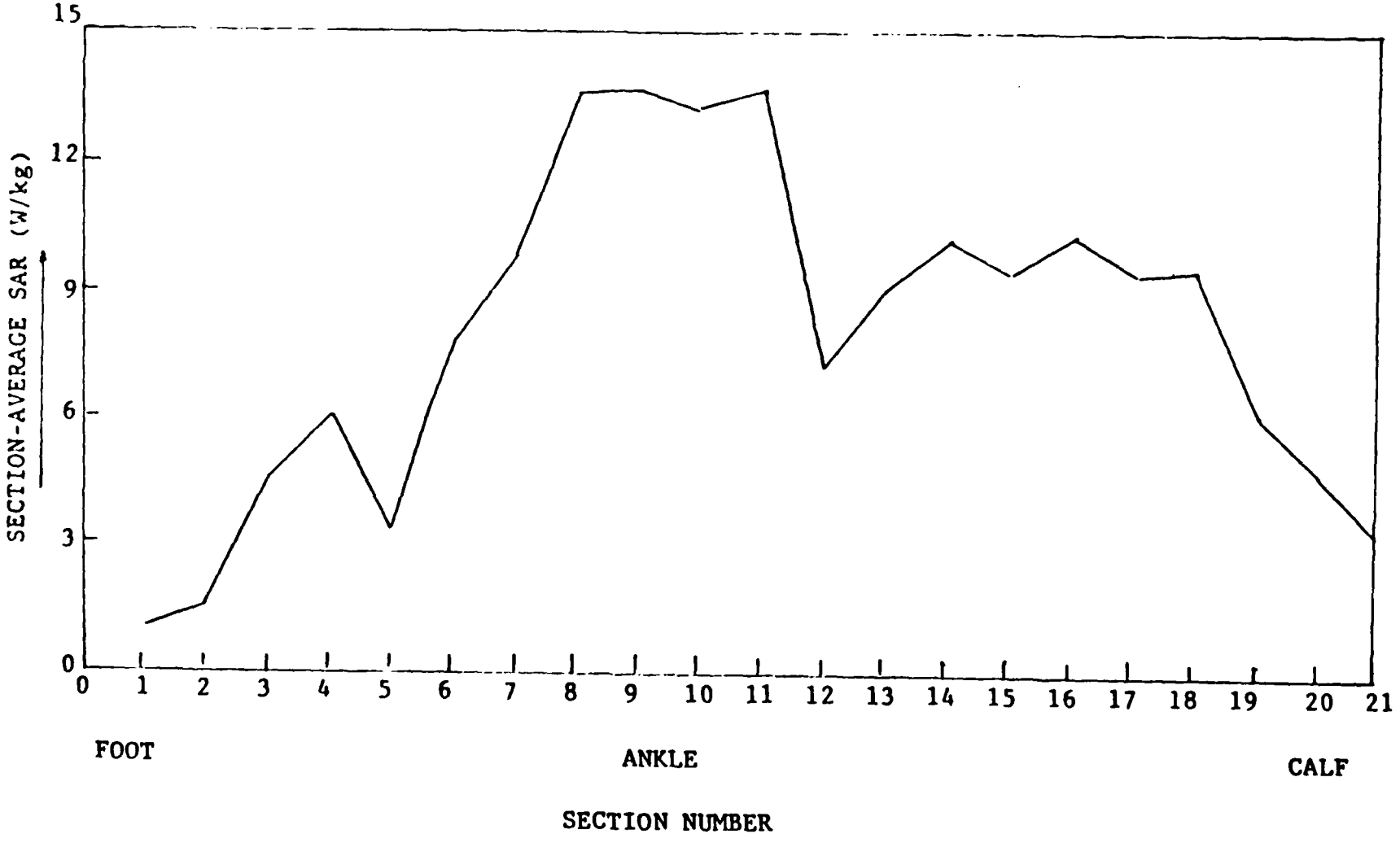

Fig. 1. Section-average electromagnetic energy deposition for 1 cm sections of the leg. I = 314 mA at 3 MHz.

1 mm^2. Finally, the EM energy deposition in the block thermal model is determined from the energy absorbed in ten different tissues in each section of the electromagnetic model. Then the heat conduction equation is applied to find the temperature distribution.

III. BLOCK MODEL AND THE HEAT CONDUCTION EQUATION

Even though cylinder models have been used in the past [6], we have formulated a block model for the heat conduction equation in order to incorporate the detailed SAR distribution under electromagnetic exposure conditions. Due to the fact that localized electromagnetic energy deposition is very difficult to obtain in the cylindrical model, the block thermal model is used to account for such deposition. The complete block thermal model is composed of 1532 cubical cells. The weight of the model is 1.22 kg. The cells are of dimension 1 cm cube for which the parameters are obtained from the inhomogeneous volume-averaged tissue properties like thermal conductivity, specific heat, blood-flow rate and metabolic heat production. These parameters are obtained from the physiological literature [5, 18-21] for 13 different tissues as shown in Table 2.

The percentage of the different tissue types in each cell of the model is determined from the anatomy handbooks [13,22]. The volume-weighted average values of the physiological parameters in one centimeter sections are determined by linear interpolation. Total basal metabolic heat production for the leg model is found to be 0.35 W and the total blood flow in the model is determined to be 1.988 ℓ/hr. These values are consistent with the literature [6].

Table 2. Different tissue properties for the thermal model.

Tissue type	Density Units of 10^3 kg/m^3	Specific heat Whr/°C kg	Thermal conductivity W/°C m	Blood flow rate ℓ/min.kg	Metabolic rate W/kg
Air	0.001	0.28	0.00925	0	0
Dry bone and ligament/tendon/ connective tissue	1.28	0.54	0.69	0.005	.02
Fat/yellow marrow	0.85	0.64	0.21	0.02	0.23
Muscle	1.05	1.05	0.642	0.0275	0.67
Red marrow/brain	1.05	1.03	0.528	0.02	0.32
Tendon/ligament/ connective tissue	1.05	0.64	0.21	0.01	0.004
Dry bone and yellow marrow	1.2	0.54	0.69	0.01	0.02
Fat and skin	0.925	0.85	0.275	0.063	0.5
Tendon/ligament/ connective tissue and muscle	1.05	0.85	0.43	0.019	0.34
Tendon/ligament/ connective tissues and fat	0.95	0.64	0.21	0.015	0.015

The transient heat conduction equation [10] which is solved for the thermal response of the block model is given by (5).

$$\rho_i c_i \frac{\partial T_i}{\partial t} = \nabla (k_i \nabla T_i) + h_{mi} + h_{emi} - h_{ei} - h_{radi} - h_{convi} + Q_{bi} (T_b - T_i) \quad (5)$$

The significance of the different parameters is discussed in the appendix.

The steady-state temperatures obtained in the peripheral cells of the model are weighted average temperatures over the volumes of the cells. The peripheral cells contain a substantial amount of air and as a result the volume-average thermal conductivities of the cells are found to be very small which prevented the normal heat flow from the internal section of the model. This is overcome by assuming the thermal conductivities of the cell to be averaged over the tissue types of the cell. The same approach is adopted for the specific heat of the peripheral cells. The surface area of the thermal block model is larger than the Dubois surface area of a standard man. For this reason, some multiplier factors are introduced which account for the larger surface area of the thermal model by decreasing the effective surface area for the heat exchange terms to values given in [23,24]. For this purpose the model is considered in two separate sections, one is the lower section of the leg (up to the ankle) while the other is the foot. The constants are taken as the ratio of the Dubois surface area to the model area for each of these sections.

IV. SOLUTION OF THE HEAT CONDUCTION EQUATION AND RESULTS.

The heat conduction equation is solved in rectangular coordinates by a method which is a modification of the Douglas and Rachford [25] that achieves higher-order accuracy of the Grank-Nicholson formulation. The unconditionally stable system similar to that of Douglas and Rachford method had the advantage of using larger time steps, while the unknown temperatures are computed explicitly at the advanced time level, similar to that in the Grank-Nicholson formulation having higher-order accuracy. As a result with reduced computational time reasonable accuracy is attained. The SOR method is used for rapid convergency of the steady-state solution. The equation is solved using the HP1000 computer.

For steady-state temperature distributions under basal condition, sweating is neglected. The calculated layer-average basal temperature distributions are shown in Fig. 2. Heat transfer at the bottom of the model is assumed to occur through a shoe having high insulation [23]. The lower temperature region near the bottom of the foot is because of the extremity. The gradient inversion near the layer 4 in Fig. 2 is because of the fact that the presence of the shoe is considered up to the layer 3. Also, this physical dimension of the model near these sections sharply reduces; as a result, there are more peripheral cells containing a large percentage of air. At the top section of the model heat transfer is assumed to occur only through blood at 35.8° C. The sudden sharp fall in the upper section may be due to the truncated boundary of the model.

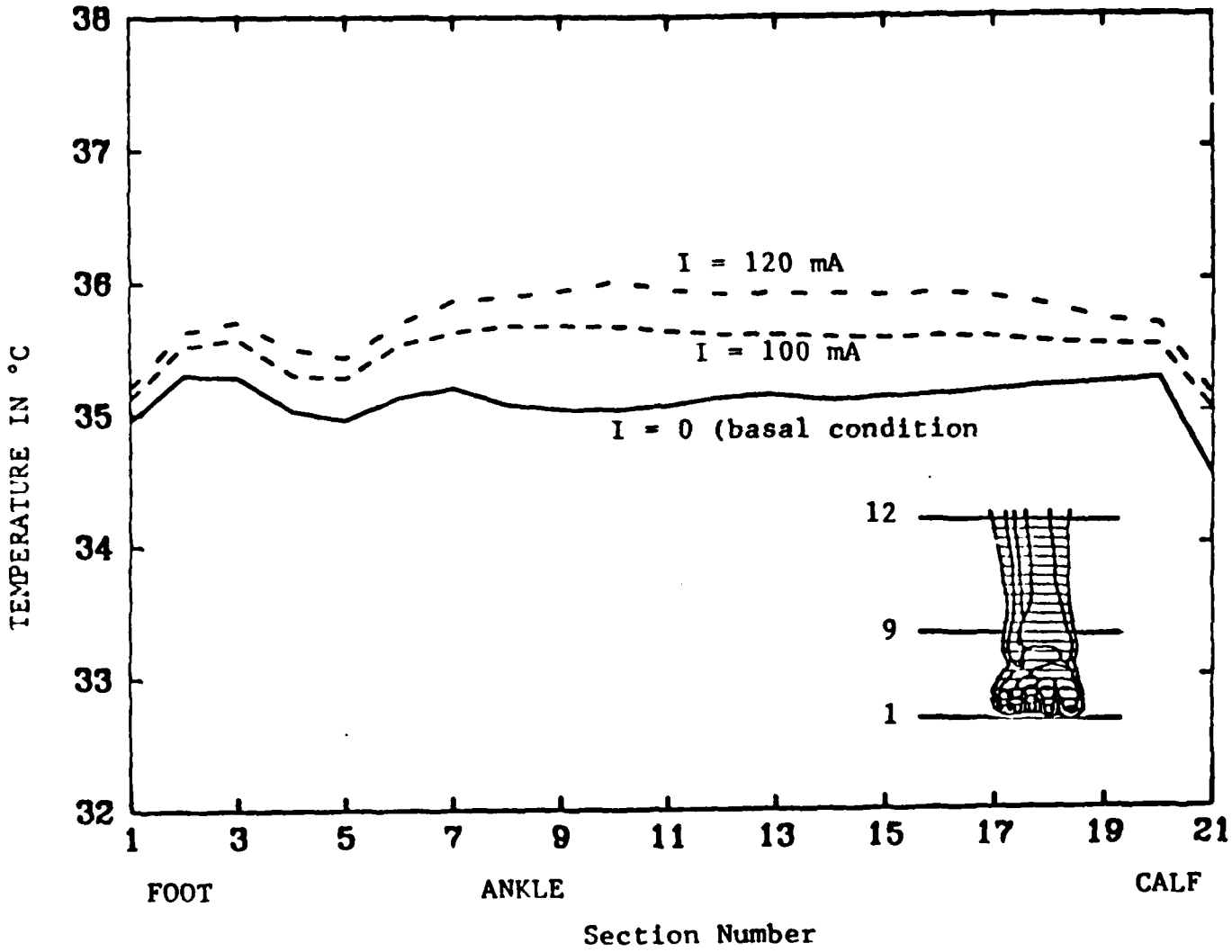

Fig. 2. Section-average temperature distribution in the lower leg section under basal conditions (I=0) and for I = 100 mA, and I = 120 mA; f = 3 MHz.

After obtaining basal temperatures, temperature distributions under electromagnetic energy depositions at one-tenth of the ANSI-recommended power density levels is determined. The current under this condition is 100 mA at 3 MHz. Layer-average-temperature rise with respect to the corresponding basal values is also shown in Fig. 2. Consistent with some preliminary experiments with a human subject, sweating is neglected under these conditions as well. It is observed that at 100 mA current (f=3 MHz) the maximum rise in temperature is found to be 0.6°C near the ankle region, while at 120 mA current (f=3 MHz) the rise in temperature is found to be about 1.0°C. The heat balance for a number of RF current flow conditions is shown in Table 3.

Temperature distributions are also obtained for electromagnetic energy depositions projected for the present ANSI Standard [1]. The RF currents projected for each of the legs are 314 mA at 3 MHz and 390 mA at 40 MHz, respectively [3]. For these conditions, sweating is included for the peripheral cells. Also, the increase in the blood-flow rate and basal metabolism is taken into account. The heat loss by sweating in the ith cell is represented by [6,23,24]

$$S_W = h_e A_{eff} (P_{Wcl} - P_{Wamb}) \tag{6}$$

h_e = Evaporative coefficient of heat transfer

P_{Wcl} = Partial pressure of saturated water vapor on clothing.

P_{Wamb} = Partial pressure of water vapor (at 50%/RH at 30° C.)

Also, the increase in blood-flow rate for the internal tissues at higher temperatures (above 39°C) is given by the linear relation as

Table 3. Heat balance table for basal and EM energy deposition condition in the leg section.

RF current in mA	Frequency in MHz	EM energy deposition	Power supplied (in W) by		Power loss (in W) due to			
			Blood	Metabolism	Radiation	Convection	Insensible perspiration	Sweating
0 (Basal Condition)			1.44	0.348	0.98	0.465	0.28	0
100	3	0.95	0.687	0.35	1.04	0.5	0.32	0
120	3	1.38	0.38	0.352	1.07	0.52	0.35	0
124	40	1.34	0.46	0.352	1.06	0.51	0.35	0
314	3	9.5	-0.1*	0.409	0.68	0.34	0.23	7.35
390	40	12.85	-3.0*	0.485	0.73	0.35	0.24	7.84

* The negative values are due to the heat carried away by the blood under the conditions of high RF currents.

follows [10]

$$Q_{dilat} = B_f \qquad \text{for } T_i < 39$$
$$Q_{dilat} = B_f\,[1 + 0.8\,(T_i - 39)] \qquad \text{for } 39°C < T_i < 44°C$$
$$Q_{dilat} = 5\,B_f \qquad \text{for } T_i > 44°C \qquad (7)$$

where

Q_{dilat} = Increased blood flow ℓ/hr

B_f = Basal blood flow ℓ/hr

From physiological considerations, upper limits have been taken for both, the heat loss by sweating and the increase in blood-flow rates. The maximum rate of sweating depends on the water vapor pressure in air, water vapor pressure at the skin and the rate of convective heat transfer. The blood-flow rates in the peripheral cells are assumed to saturate at somewhat higher values than the internal tissues and are taken to be ten times the basal values. To find the saturation values integrated output from skin, warm and cold receptors are determined [6].

The heat conduction equation is solved after introducing the heat loss by sweating and increase in blood-flow rate and metabolism. Table 3 indicates that a reasonably good heat balance occurs for all of the cases that are considered. The average rise in temperature for 314 mA (at 3 MHz) and 390 mA (at 40 MHz) in each section of the model is shown in Fig. 3. The figure indicates that for the prescribed currents the highest average increase in temperature is 3.8°C and 4.85°C for 314 mA and 390 mA, respectively, near the ankle region. It may be mentioned here that from Fig. 1 the EM energy deposition is found to be highest in these sections as well.

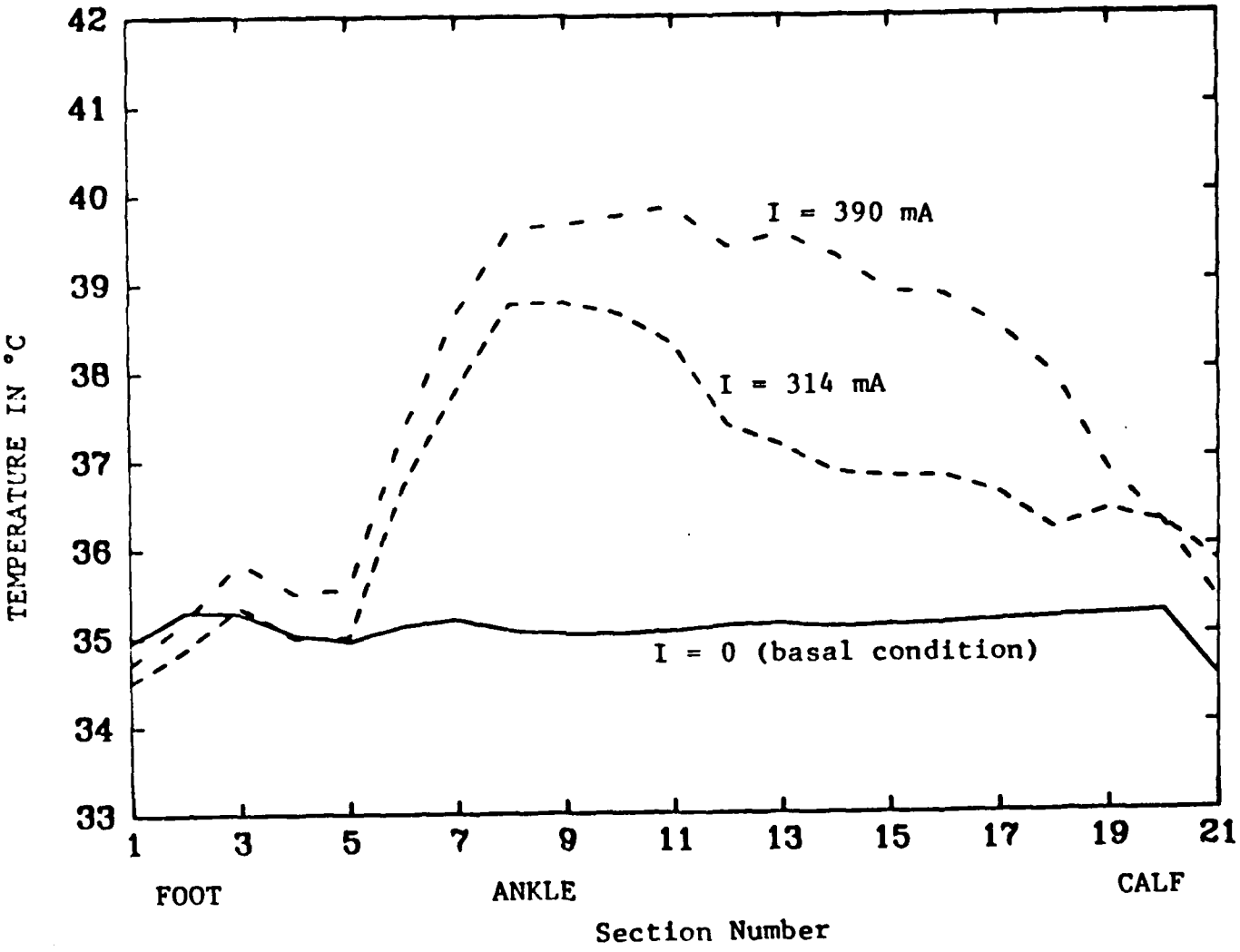

Fig. 3. Average temperature distribution in the lower leg section for RF currents of 314 mA (f = 3 MHz) and 390 mA (f = 40 MHz).

For clarity of presentation, temperature distribution in one of the sections near the ankle region is shown in Fig. 4(b). For comparison, the basal temperature in that section is also given in Fig. 4(a). The hot spots are found to exist in the internal region of the section. This is because of the presence of highly-conducting tissues like synovial fluid, periostium, red marrow (present inside small bones [26]) and muscle which results in high EM energy in these tissues. Because of the fact that some of these tissues have thermal conductivities which are not commensurately high (see Table 2) and some are placed in the interior region (e.g., posterior tibial muscle in Fig. 4(a,b)), the generated heat is diffused to the surrounding cells at a lower rate. Therefore, this results in higher temperature under steady-state condition. Also, a smaller physical cross section for this part of the model (ankle region) is partially responsible for high SAR values. It may be observed that the temperature at the frontal part of the section in Fig. 4(b) is higher than that in the rest of the peripheral area. This is because this portion of the section is composed of highly-conducting tissues like periostium (surrounding the tibia and fibula), synovial fluid (present between the tibia and fibula), anterior tibial muscle and red marrow (present inside the bones). As a result, high SARs are deposited in this part of the section which culminates in increased temperature. The high rise in temperature in these sections causes the blood flow to increase appreciably. The increased blood flow due to vasodilation at 314 mA (f = 30 MHz) is shown in Fig. 5. It indicates that blood flow increases to about six to seven times its basal values in these section.

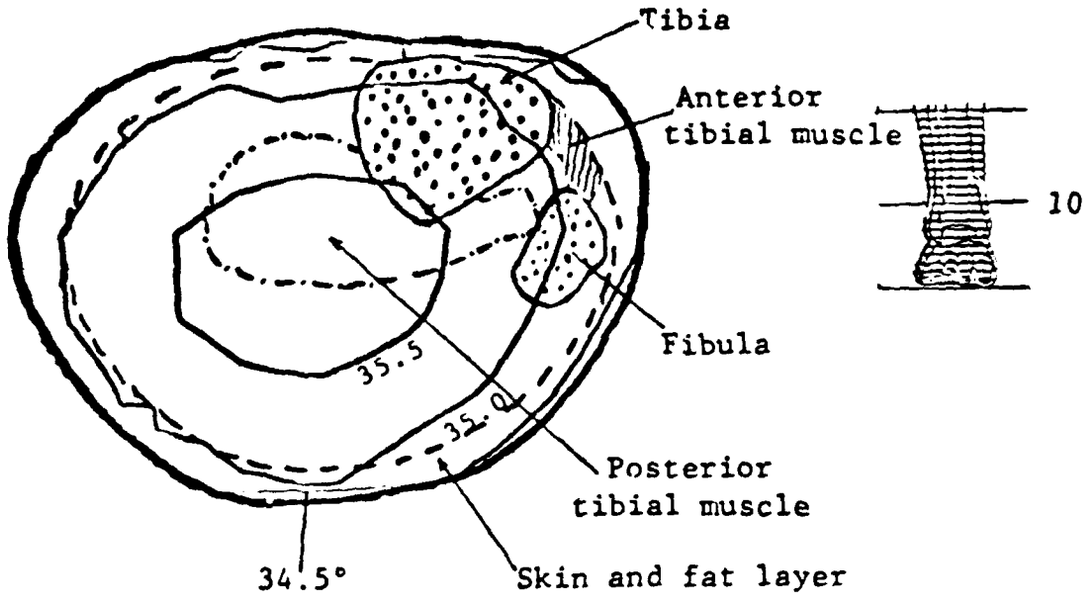

(a) For basal condition without RF current.

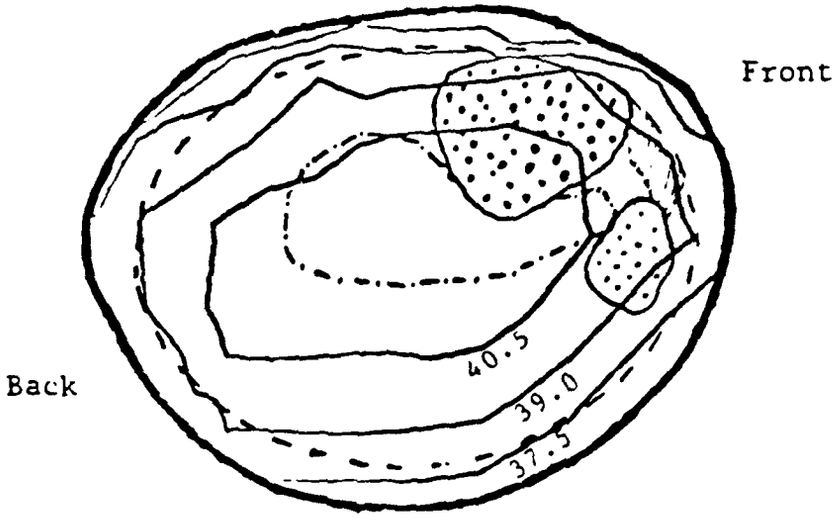

(b) At I = 314 mA (f = 3 MHz)

Fig. 4. Contours of constant temperature (°C) for Section 10 of the model near the ankle region.

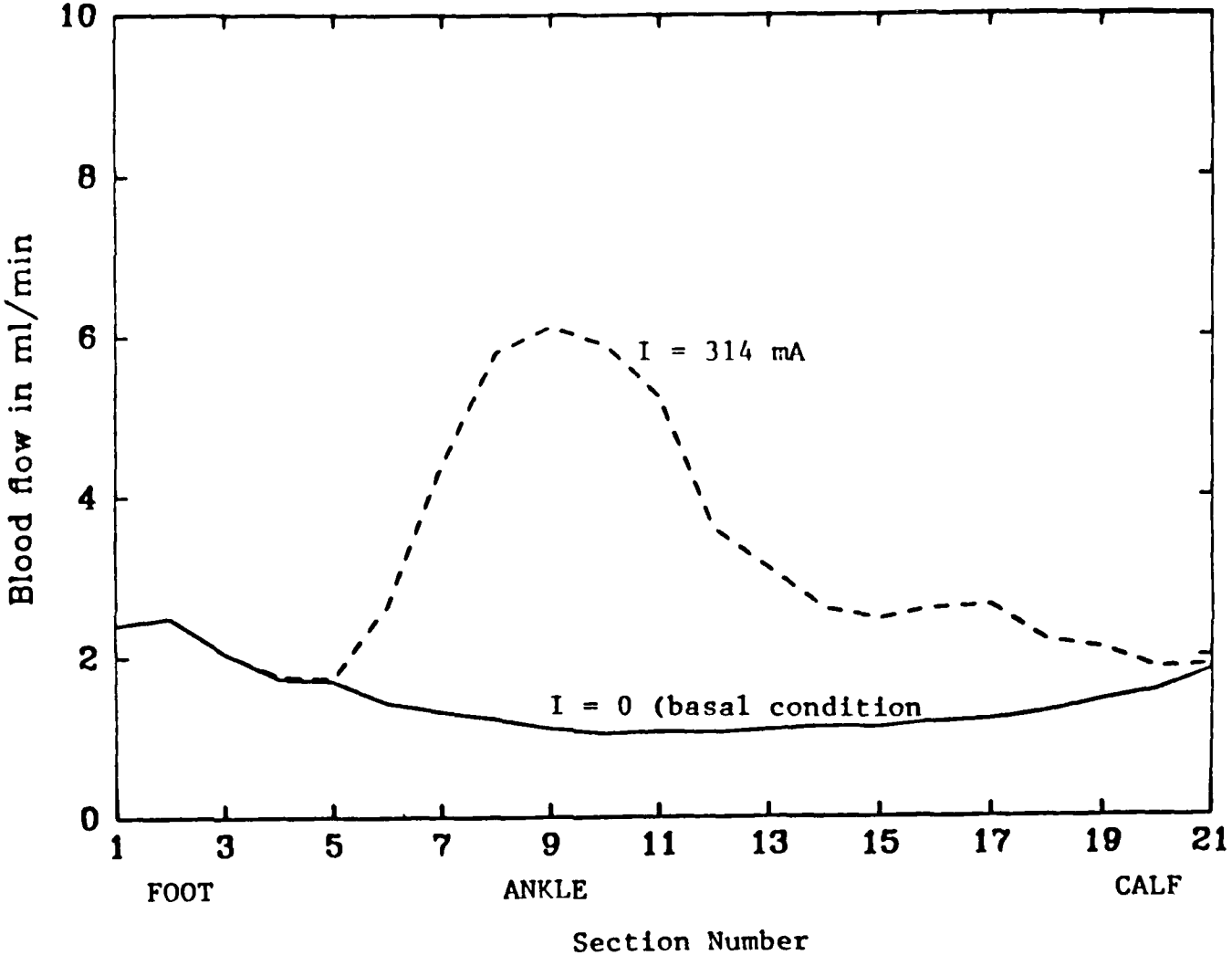

Fig. 5. Average blood flow in the leg section for an RF current of 314 mA at 3 MHz.

It is observed from Fig. 3 that the average temperatures for the lowest sections of the model are slightly less than the basal temperatures. This is because of the presence of sweating which results in a drop in the skin temperature. This decrease in the skin temperature as a result of sweating has been reported previously in the literature [27,28]. The curves shown in [27] indicate that under sweating condition the mean-skin-temperature of the subject can drop to as low as 30°C from a nonsweating temperature of 34.5°C.

IV. TRANSIENT SOLUTION AND COMPARISON WITH EXPERIMENTS

In order to compare the behavior of the model with that of the recent experiments [29], transient response of the model is determined at 5 and 40 MHz for three minutes and eight minutes of irradiation, respectively. The point taken for comparison is at the front of the leg at the ankle section (see inserts of Figs. 6 and 7) which corresponds to the region of maximum superficial heating [29] under conditions of RF current flow. Since the initial temperature buildup did not produce any observable sweating, the thermal model also did not consider the sweating during the first few minutes. Since the experiments of eight minutes duration (limited in time by physical discomfort) indicates an initiation of sweating after about seven minutes [30], we too have introduced such a loss in our model. A delay in the sweating may be because the full response of the sweat glands requires a finite time interval to attain its full activation level. The results of the calculations under transient conditions are shown in Figs. 6 and 7. Since the exposure time in Fig. 6 is less than seven minutes, sweating

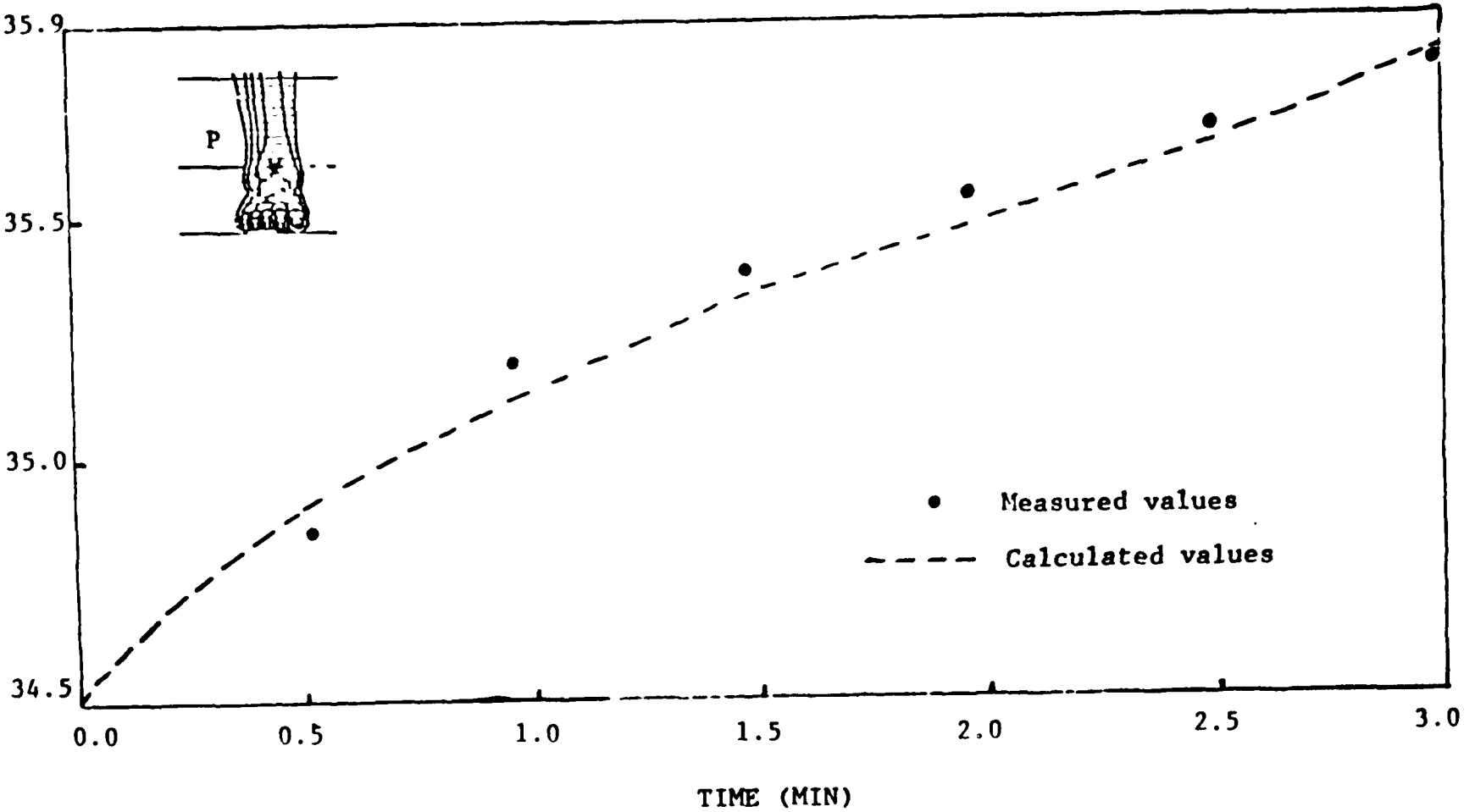

Fig. 6. Comparison between the measured temperature and the calculated values for point P of the ankle region. f = 5.0 MHz, I = 275 mA.

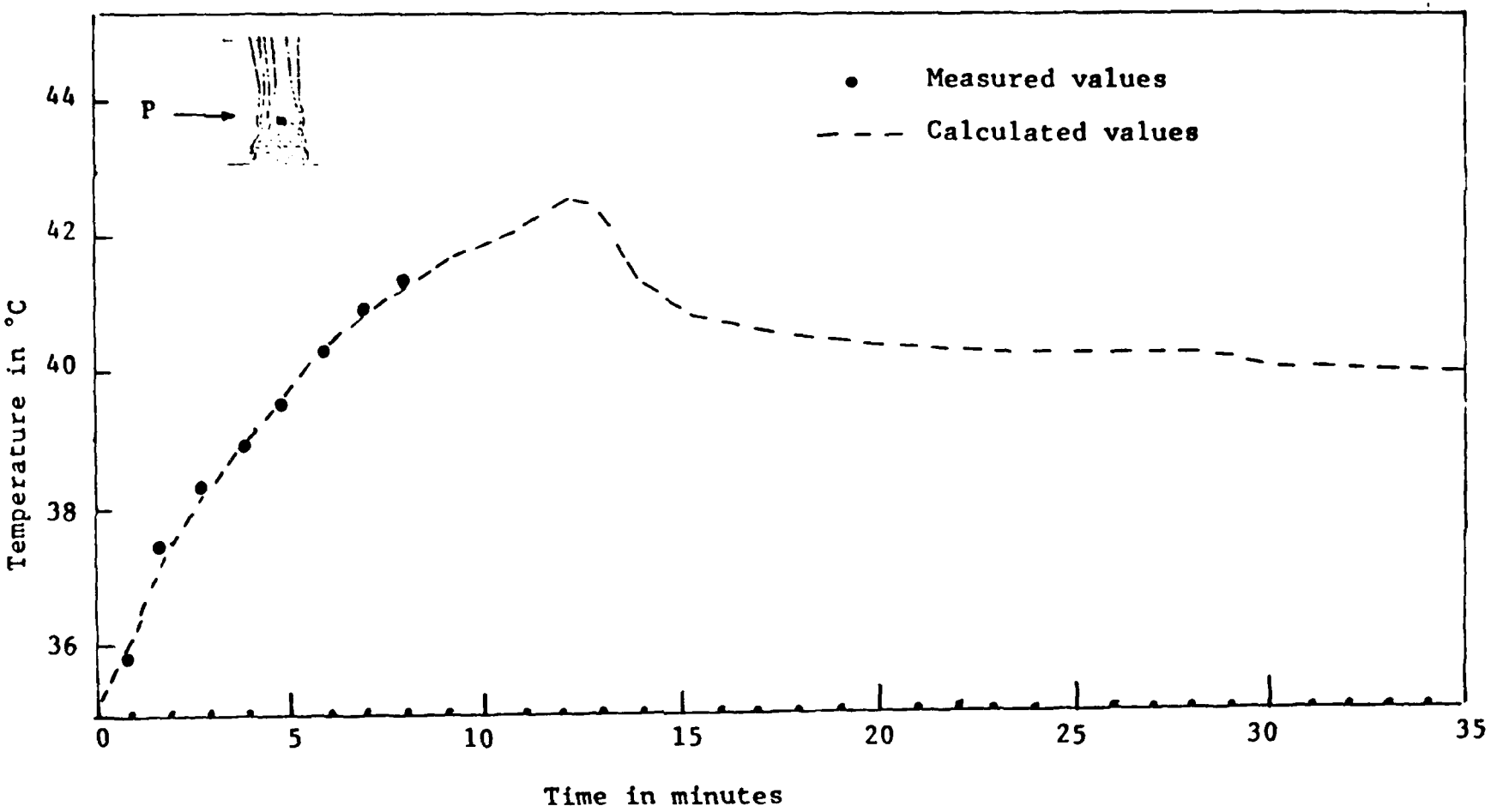

Fig. 7. Comparison between the measured temperature and the calculated values for point P of the ankle section. f = 40 MHz, I = 399 mA.

is not considered in the calculations. It may be noticed in Fig. 7 that the surface temperature attains a maximum value of about 42.6°C, then it gradually reaches to its steady-state value. The sharp drop in temperature after about 12 minutes is due to increased blood flow and sweating.

VI. MODEL DRAWBACKS

It should be realized that the model has some deficiencies in different aspects. The cell size of the thermal model is taken to 1 cm cubes, which indicates the volume average properties of the tissues. For this reason, some of the tissues such as periostium, synovial fluid, skin, which are considered for the electromagnetic model (with 1 mm^2 resolution), cannot be taken into account properly in the thermal model. Again, lack of proper modeling of the skin (which is responsible for the total heat exchange of the model with environment) has introduced some limitations on the model performance. It is observed that most of the peripheral cells contained more than 75 percent air which resulted in lowering of the overall temperature of these cells. The effect on heat flow because of this deficiency, however, is corrected by taking the values of heat conductivities and specific heats corresponding only to the volume-averaged properties of the biological tissues in the peripheral cells. Since we used 1 mm^2 resolution in the cross-sectional planes for the electromagnetic model, the detailed SAR calculations are relatively free from the large cell size problems. As it is not possible to obtain the anatomical cross sections with less than 1 cm spacing, the electromagnetic model is obtained by connecting

21 equivalent impedances in series with each other. It has been mentioned earlier that there is a slight variation of the impedance obtained from this model as compared to the experimental results obtained by Guy, et al. [17]. This is because of the finite thickness of the various sections used for the model.

VII. DISCUSSION

This paper describes an inhomogeneous block thermal model of the lowest 21 cm of the human leg consisting of 1532 cells each 1 cubic cm in size. The object of this model is to study the temperature distribution in the lowest part of the leg for conditions of electromagnetic exposure prescribed by the present ANSI Standard. Two analyses are performed in particular. These are for 314 mA at 3 MHz, and 390 mA at 40 MHz -- currents that may be set up in the human leg [3,4] for E-fields recommended by the present ANSI Standard. Fig. 3 indicates that average increases in temperature for the ankle section under these conditions are 3.8°C and 4.85°C, respectively. Both temperature profiles indicate much similarity. The region of high temperature is near the ankle. The blood-flow rate increases substantially under these conditions (Fig. 5).

The heat supplied by the blood is found to vary under these conditions. At 314 mA (f=3 MHz) 0.1 Watt of heat is taken by the blood in contrast to 1.4 Watt heat supplied by the blood under basal condition. At 390 mA it was observed that 3.01 Watt of heat is supplied to the blood from the leg model under consideration. The increase in metabolism is also indicated in Table 3. Studies are also made to find

the temperature distribution of the model with EM power deposition for incident power densities roughly one tenth of those given by the present ANSI guideline. As observed by a subject experimentally, sweating is neglected under these conditions. The RF currents used are 100 mA at and 120 mA at 3 MHz, respectively. The section-average temperatures rose about 0.6°C and 1.0°C, respectively, for the ankle region. These results are in good agreement with the experimental data [29]. Lower temperature increases are calculated for the rest of the leg sections. Transient solutions of the model are compared with the experimental data for the initial increases in temperature near the ankle region. Numerical results at 399 mA indicate a sharp rise in temperature up to 42.6°C after about 10 minutes of irradiation. The results are consistent with the experimental data. Increased blood flow and sweating causes the temperature to eventually attain a steady-state value of 39.5°C. As the behavior of the sweat glands under transient conditions is not exactly known, the curve shown in Fig. 7 may have to be modified somewhat, according to the performance characteristics of the sweat glands.

ACKNOWLEDGMENT

The authors gratefully acknowledge the many useful discussions with Professor J. L. Lords and Dr. Shaukat Jahan of the University of Utah. This work was supported by the Office of Naval Research under Contract N00014-86-K0104.

REFERENCES

1. ANSI C95.1 - 1982, "American National Standard-Safety levels with respect to human exposure to radio frequency electromagnetic fields, 30 KHz to 100 GHz," IEEE, New York.

2. American Conference on Governmental Industrial Hygienists, "Threshold Values for 1983-1984," Cincinnati, Ohio.

3. O. P. Gandhi, J-Y Chen and A. Riazi, "Currents induced in a human being for plane-wave exposure conditions, 0-50 MHz and for RF sealers," IEEE Transactions on Biomedical Engineering, Vol. BME-33, 1986, pp. 757-767.

4. O. P. Gandhi, I. Chatterjee, D. Wu and Y. G. Gu, "Likelihood of high rates of energy deposition in the human legs at the ANSI recommended 3-30 MHz RF safety levels," Proceedings of IEEE, Vol. 73, 1985, pp. 1145-1147.

5. J. A. J. Stolwijk, "Mathematical model of thermoregulation," in Physiological and Behavioral Temperature Regulation, J. D. Hardy, A. P. Gagge, and J. A. J. Stolwijk, Editors, Charles C. Thomas, 1970, Springfield, Illinois, Chapter 48, pp. 703-721.

6. J. A. J. Stolwijk and J. D. Hardy, "Control of body temperature," in Handbook of Physiology, Section 9: Reactions to environmental agents, Williams and Wilkins, Baltimore, Maryland, 1971, Chapter 4, pp. 44-68.

7. J. A. J. Stolwijk, "Mathematical models of thermal regulations," Ann. N. Y. Acad. Sci., Vol. 335, 1980, pp. 98-106.

8. E. H. Wissler, "Steady-state temperature distribution in man," J. Appl. Physiology, Vol. 16, 1961, pp. 734-740.

9. E. H. Wissler, "A mathematical model of the human thermal system," Bull. Math. Biophys., Vol. 26, 1964, pp. 147-166.

10. I. Chatterjee and O. P. Gandhi, "An inhomogeneous thermal block model of man for the electromagnetic environment," IEEE Trans. on Biomedical Engineering, Vol. BME-30, 1983, pp. 707-715.

11. M. J. Hagman, O. P. Gandhi, and C. H. Durney, "Numerical calculation of electromagneti energy deposition for a realistic model of man," IEEE Trans. Microwave Theory Tech., Vol. MTT-27, 1979, pp. 804-809.

12. D. Sullivan, O. P. Gandhi and Taflove, "Use of the finite-difference time-domain method in calculating EM absorption in man models," to be published.

13. W. J. Bo, J. Meschon, and W. A. Kruger, Basic Atlas of Cross-Sectional Anatomy, 1980, W. B. Saunders Company, Philadelphia, PA, pp. 270-280.

14. C. C. Johnson and A. W. Guy, "Nonionizing electromagnetic wave effects in biological materials and systems," Proceedings of the IEEE, Vol. 60, 1972 pp. 692-718.

15. S. R. Smith and K. R. Foster, "Dielectric properties of low-water content tissues," Physics in Biology and Medicine, Vol. 30, 1985, pp. 965-973.

16. C. H. Durney, et al., Radio Frequency Radiation Dosimetry Handbook, Second Edition, 1978, Report SAM-TR-78-22.

17. A. W. Guy and C. K. Chou, "Hazard Analysis: Very low frequency through medium frequency range," Final Report, USAF SAM Contract F36615-78-D-0617, Task 0065, 1982.

18. J. A. J. Stolwijk and J. D. Hardy, "Temperature regulation in man - a theoretical study," Pfluger's Arch. Gesamte Physiol. Menschen Tiere, Vol. 291, 1966, pp. 129-162.

19. A. C. Guyton, Texthook of Medical Physiology, Sixth Edition, P. A. Saunders, Philadelphia, 1981.

20. V. J. Aschoff and R. Weven, "Kern and schale in warmehausholt des menschen," Die Naturwissenschaften, Vol. 45, 1958, 477-485.

21. M. Lipkin and J. D. Hardy, "Measurement of some thermal properties of human tissues," J. Appl. Physiol., Vol. 7, 1954, pp. 212-217.

22. G. J. Tortora and N. P. Anagnostakos, Principles of Anatomy and Physiology, Third Edition, Harper and Row Publishers, New York, 1971, pp. 3-30, 219-230, 173-190.

23. P. O. Fanger, "Conditions for thermal comfort. Introduction of a general comfort equation," in Physiological and Behavioral Temperature Regulation, J. D. Hardy, A. P. Gagge, and J. A. J. Stolwijk, Editors, Charles C. Thomas, Springfield, Illinois, 1970, Chapter 11, pp. 152-176.

24. A. P. Gagge and Y. Nishi, "Heat exchange between human skin surface and thermal environment," in Handbook of Physiology, Section 9: Reactions to environmental agents, Williams and Wilkins, Baltimore, Maryland, Chapter 5, pp. 69-92.

25. P. L. T. Brian, "A finite-difference method of high-order accuracy for the solution of three-dimensional transient heat conduction problems," A. I. Ch. E. Journal, Vol. 7, No. 3, 1961, pp. 367-370.

26. A. W. Ham and D. H. Cormack, Histology, Eighth Edition, 1979, J. B. Lippincott Company, Chapter 12, p. 307.

27. P. O. Fanger, "Calculation of thermal comfort: Introduction of a basic comfort equation," presented at the ASHRAE 74th Annual Meeting, Minneapolis, Minnesota, 1967.

28. D. F. Brebner, D. Mek Kerslake, and J. L. Waddell, "The diffusion of water vapor through human skin," J. Physiology, 1956, 132:225-231.

29. J. Y. Chen and O. P. Gandhi, "Thermal implications of high SARs in the body extremities at the ANSI recommended VLF-VHF safety levels." Submitted to IEEE Transactions on Biomedical Engineering.

30. J. Y. Chen - personal communication.

APPENDIX

The Bioheat Equation

The transient bioheat equation [10] which is solved for the thermal response of the block model is given by

$$\rho_i c_i \frac{\partial T_i}{\partial t} = \nabla (K_i \nabla T_i) + h_{mi} + h_{emi} - h_{ei} - h_{radi} - h_{convi} + Q_{bi} (T_b - T_i) \quad \text{(A-1)}$$

T_i = Instantaneous temperature of the cell (°C)

ρ_i = Mass density of the ith cell (kg/m^3)

c_i = Specific heat of the ith cell [Whr/(°C kg)]

k_i = Thermal conductivity of the cell [W/(°C m)]

h_{mi} = Metabolic heat generation/unit volume (W/m^3). (Varies with the rise of temperature.)

h_{emi} = Electromagnetic energy deposition/unit volume (W/m^3)

h_{ei} = Evaporative heat dissipation in the peripheral cells/unit volume (includes sweating and insensible perspiration) (W/m^3)

h_{radi}, h_{conv_i} = Radiative, convective heat loss from the peripheral cells/unit volume (W/m^3)

Q_{bi} = Product of mass flow rate, density and specific heat of capillary blood in the tissue [$W/(m^3$ °C)]

T_b = Temperature of arterial blood entering the tissue assumed to be at 35.8°C.

It is assumed that heat exchange between blood and tissue occurs in the capillaries only [5,10]. The boundary conditions are introduced in the peripheral cells by the loss terms as h_{rad}, h_{conv_i}, and h_{ei}. The empirical equations for these loss terms have been obtained from studies by Fanger [23] and Gagge and Nishi [24] for clothed body. These are given in the following:

$$h_{radi} = A_{eff}\ \acute{\varepsilon}\delta\ [(T_{c\ell} + 273)^4 - (T_i + 273)^4] \text{ (K cal/hr)} \qquad \text{(A-2)}$$

$$h_{conv_i} = A_{Du}\ f_{c\ell}\ h_c\ [T_{c\ell} - T_i] \text{ (K cal/hr)} \qquad \text{(A-3)}$$

$$h_{PD} = 0.35\ A_{Du}\ (1.92\ T_i - 25.3 - P_a) \text{ (K cal/hr)} \qquad \text{(A-4)}$$

$$h_{mi} = h_{mib}\ (1.1)^{\Delta T} \quad W/m^3 \qquad \text{(A-5)}$$

$$T_{c\ell} = T_a + F_{c\ell}\ (T_i - T_a) \quad °C \qquad \text{(A-6)}$$

$$F_{c\ell} = I_o/I_o + I_{c\ell}) \qquad \text{(A-7)}$$

$$A_{eff} = f_{eff}\ f_{c\ell}\ A_{Du} \qquad \text{(A-8)}$$

where,

A_{eff} = Effective area of the clothed body.

f_{eff} = Ratio of the effective radiation area of the clothed body to the surface area of the clothed body = 0.65 (for seated person).

$f_{c\ell}$ = Ratio of the surface area of the clothed body to the nude body.

A_{Du} = The Dubois area.

h_{mib} = Basal metabolic heat production.

h_c = Convection coefficient.

= $2.05\ (T_{cl} - T_a)^{.25}$. (K cal/$m^2$-hr-°C)

δ = Stefan-Boltzman constant = 5.67×10^{-8} W m^{-2} K^{-4}.

ϵ' = Emissivity of skin = 1.

P_a = Partial pressure of water vapour in the ambient air.

T_{cl} = Clothing temperature.

$\Delta T = T_i - T_{ib}$

T_{ib} = Temperature of the ith cell under basal condition.

T_a = Ambient temperature (30°C).

F_{cl} = Thermal efficiency factor.

I_o = Thermal resistance of operating environment.

I_{cl} = Effective insulation of clothing.

END

DATE

FILMED

6-1988

DTIC